ON THE TRANSFORMATION MECHANISMS AND THE PREDICTION OF FINITE-DEPTH WATER WAVES

By

SHU-CHI VINCENT HSIAO

A DISSERTATION PRESENTED TO THE GRADUATE COUNCIL
OF THE UNIVERSITY OF FLORIDA
IN PARTIAL FULFILLMENT OF THE REQUIREMENTS FOR THE
DEGREE OF DOCTOR OF PHILOSOPHY

UNIVERSITY OF FLORIDA

1978

ACKNOWLEDGMENTS

I am indebted to Professor Omar H. Shemdin for his supervision and support during the course of this work.

I owe my thanks to Professor Klaus Hasselmann and Dr. Klaus Herterich for their assistance and valuable discussions.

Dr. J. Ernest Breeding, Jr., is sincerely acknowledged for having provided the Panama City wave data and useful discussions.

I wish to thank Ms. S. Lyn Bayley for her proofreading and suggestions.

This work was supported by the State of Florida through a Special Grant to the Coastal and Oceanographic Engineering Laboratory. The analysis was partially supported by the Office of Naval Research, Geography Branch, under Contract Number N 00014-76-MP60029.

TABLE OF CONTENTS

TABLE OF CONTENTS (Continued)

LIST OF FIGURES

LIST OF FIGURES (Continued)

LIST OF FIGURES (Continued)

Abstract of Dissertation Presented to the Graduate Council of the University of Florida in Partial Fulfillment of the Requirements for the Degree of Doctor of Philosophy

ON THE TRANSFORMATION MECHANISMS AND THE PREDICTION OF FINITE-DEPTH WATER WAVES

By

Shu-Chi Vincent Hsiao

June, 1978

Chairman: Omar H. Shemdin
Major Department: Engineering Sciences

The finite-depth water wave transformation mechanisms are discussed in this dissertation. These include wind generation, wave breaking, nonlinear energy transfer, bottom friction, percolation, wave-soft bottom interaction, refraction, and shoaling. A prediction model is developed using the wave energy equation and the above wave transformation mechanisms. The mathematical formulation for each mechanism is either derived in this dissertation or constructed based on updated theories and experiments. The comparisons between model computations and field measurements show good agreement.

CHAPTER I

INTRODUCTION

In recent years, there has been a rapid increase in the development of human activities in coastal and nearshore areas. A variety of these activities require the use of a finite-depth water wave prediction model. Better knowledge of the shallow water wave climate will aid in locating and exploiting offshore resources, such as oil and gas. It is an essential input for the design and construction of coastal and nearshore structures. A shallow water wave prediction capability is of benefit to navigation, nearshore fisheries, and water sports and recreation. Moreover, wave information is imperative in any quantitative analysis of coastal processes.

There have been many studies on the topic of wave prediction. In 1947, Sverdrup and Munk developed the significant wave method. The significant wave height is the mean of the highest one-third of all waves present in a wave train and has been shown to be nearly equal to wave heights reported from visual observations. This method predicts waves by using the empirical relationships between windspeed, fetch length, wind duration, significant wave height, and significant wave period. It is still being used because of its simplicity. Later, in 1955, Pierson, Neumann, and James developed the "wave spectrum method." It predicts waves by using the empirical relationships between windspeed, fetch length, wind duration, wave energy, and peak frequency.

However, since both methods are purely empirical, not much wave theory was used as needed for a deterministic approach.

With new advances in the understanding of wave theories, complemented by the increased amount of wave data available and the processing capabilities of computers, more sophisticated wave models have been developed. Pierson, Tick, and Baer (1966), Inoue (1967), Lazanoff, Stevenson, and Cardone (1973), and Salfi (1974), as well as Cardone, Pierson, and Ward (1976) all applied the wind generation theories developed by Miles (1957) and Phillips (1957) to their models. The nonlinear wave energy transfer theory developed by Hasselmann (1962, 1963a, 1963b) was incorporated into the models produced by Barnett (1968) and Ewing (1971). Hasselmann, Ross, Müller, and Sell (1976) applied the shape stabilizing influence of nonlinear energy transfer in developing their parametric model. However, all of these models are for deep water ocean wave prediction where the important mechanisms are wind generation, wave breaking, and nonlinear wave energy transfer. These models cannot be applied in shallow water areas, such as the inner continental shelf, because the wave transformation mechanisms of refraction, shoaling, bottom friction, bottom percolation, and soft bottom interaction are also important mechanisms in addition to what was previously mentioned.

Collins (1972) has been the only investigator so far to develop a model for shallow water wave spectral prediction. His model included the mechanisms of generation, breaking, refraction, shoaling, and friction; but nonlinear transfer, percolation, and soft bottom interaction were not considered.

In this dissertation, a shallow water wave prediction model is developed using the most current wave theories. For a given deep water

spectrum, the evolution of the spectrum is calculated as waves propagate toward shore before reaching the surf zone where the waves become highly nonlinear. It includes the wave transformation mechanisms of generation, breaking, nonlinear interaction, refraction, shoaling, friction, percolation and wave-soft bottom interaction. In order to simplify the numerical computations, the bottom contours are assumed to be straight and parallel, an acceptable approximation in many areas.

The predictions and wave measurements are compared for waves off Marineland, Florida; Panama City, Florida; Melkbosstrand, South Africa; an area offshore of the Middle Atlantic states; and East Bay, Louisiana. Satisfactory comparisons between predictions and measurements were obtained in all the cases tested.

CHAPTER II

RECENT ADVANCES RELATED TO WAVE GENERATION AND NONLINEAR WAVE ENERGY TRANSFER

There have been many studies on the problem of wave generation. A review and an assessment of those studies are given in this chapter.

II.A. Wave Generation

1. Theories

Two basic mechanisms for the wind generation of waves were proposed separately, one by Phillips (1957) and the other by Miles (1957, 1959). Phillips considered the generation of waves by normal pressure fluctuations due to a turbulent wind. He found the waves to grow by a resonance mechanism when the speed and length of the atmospheric pressure fluctuations match those of the water waves. His theory shows that wave energy grows linearly with time and is proportional to the spectrum of pressure fluctuations, i.e., [following Hasselmann's (1968) notation]

$$\frac{DF(\vec{k})}{Dt} = \frac{\pi\omega^2}{2\rho g} F_p(\vec{k},\omega) \quad , \tag{2-1}$$

where $\pi = 3.1416$, F is two-dimensional wave spectrum, F_p is three-dimensional atmospheric pressure spectrum, $\vec{k}$ is two-dimensional wave number, t is time, ρ is water density, and ω is wave frequency in radians per second. Phillips' mechanism is important only in bringing the wave energy from zero to certain levels at which point the

mechanism proposed by Miles becomes important. Miles' mechanism is responsible for the major portion of the energy transfer from wind to waves.

Miles considered the energy transfer from wind to waves by the wave perturbed pressure in a turbulent shear air flow. The phase lag of pressure with respect to the wave produces momentum transfer to the wave. Such an air flow pattern (Figure 1) had been measured in the laboratory by Shemdin (1969). The transfer of momentum can be demonstrated by considering a progressive sinusoidal wave defined by

$$\eta = a \exp[i(kx-\omega t)] \quad , \tag{2-2}$$

where a is wave amplitude, k is wave number, x is the horizontal coordinate, and $i = \sqrt{-1}$. The wave perturbed pressure at the water surface can be written in the form of

$$p = (\alpha + i\beta)\, \rho_a g \eta \quad , \tag{2-3}$$

where α and β are the in-phase and out-of-phase pressure coefficients respectively, ρ_a is air density, and g is gravitational acceleration. The momentum transfer from air to water is

$$M = \frac{1}{L} \int_0^L p \frac{\partial \eta}{\partial x} dx \quad ,$$

where L is wave length. After integration, it becomes

$$M = \frac{\beta}{2} \rho_a g k a^2 \quad . \tag{2-4}$$

Only the out-of-phase pressure contributes to momentum transfer. The energy transfer rate is

$$\frac{dE_m}{dt} = Mc = \frac{\beta}{2} \rho_a g \omega a^2 \quad , \tag{2-5}$$

where

$$E_m = \frac{1}{2} \rho g a^2 \quad , \tag{2-6}$$

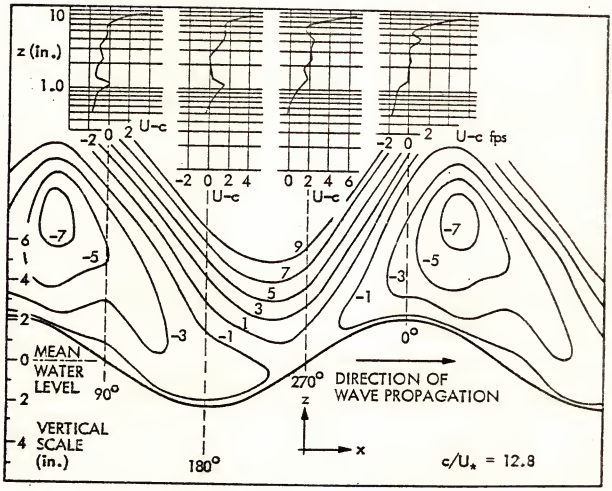

Figure 1. Wave-induced vortex pattern in the air stream over waves [After Shemdin (1969)].

is wave energy per unit surface area. Equation (2-5) can be written as

$$\frac{dE_m}{dt} = \beta \frac{\rho_a}{\rho} \omega E_m \quad . \tag{2-7}$$

The coefficients α and β can be found by solving numerically the Orr-Sommerfield equation for air flow by assuming a mean wind velocity profile. Miles' (1959) results are shown in Figure 2. By combining his and Phillips' theories, Miles (1960) found that his mechanism is dominant in the principal stage of wave development.

The effect of air turbulence on wave generation has been discussed by Phillips (1969) and Miles (1967). Davis' (1970, 1972) and Reynolds and Hussain's (1972) theoretical studies both suggested that turbulent Reynolds stresses are essential to the process of energy flow to the waves.

Townsend (1972) solved linearized equations numerically for turbulent flow over sinusoidal progressive waves by including interactions between the waves and turbulence in the air flow. He found the rate of energy transfer from wind to waves to be similar in magnitude to that given by Miles (1959). These results indicate that the energy input due to air turbulence must be relatively small. Gent and Taylor (1976) extended Townsend's work by including the nonlinear terms in the equations so that the results could be applied to larger amplitude waves. They found that the energy transfer rate is consistent with Miles' for a uniform surface roughness. However, the transfer rate can be enhanced if the surface roughness is allowed to vary along the wave.

Figure 2. Miles' theoretical results. $U_1 = 2.5\ U_*$, $\overline{\Omega} = gZ_o/U_1^2$ [After Miles (1959)].

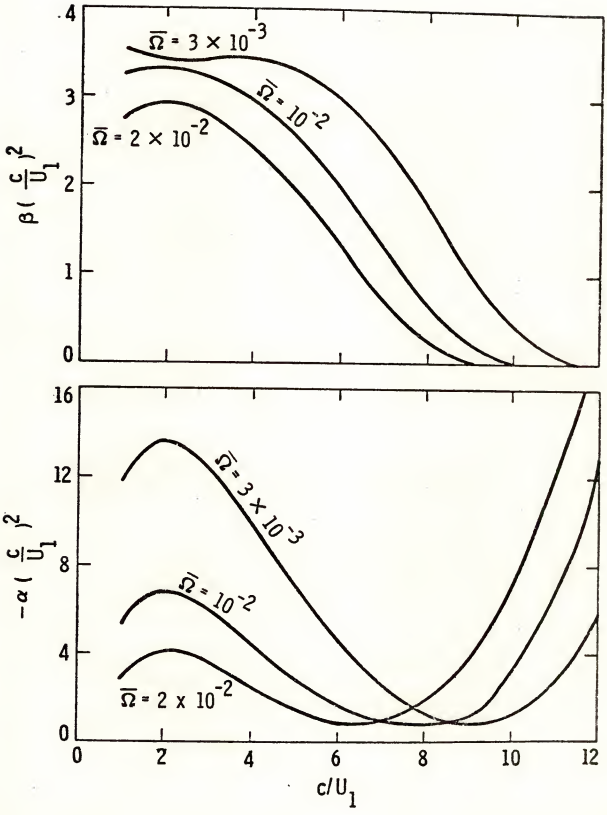
$\bar{\Omega} = 3 \times 10^{-3}$
$\bar{\Omega} = 10^{-2}$
$\bar{\Omega} = 2 \times 10^{-2}$
$\beta \left(\frac{c}{U_1}\right)^2$
$-\alpha \left(\frac{c}{U_1}\right)^2$
c/U_1
0
1
2
3
4
0
4
8
12
16
0
2
4
6
8
10
12

2. Experiments

The laboratory measurements of the coefficient β by Shemdin (1969) indicate the same order of magnitude as Miles' for $U_*/c \approx 0.15 - 0.4$, where U_* is the friction velocity defined by $\sqrt{\tau/\rho_a}$ and τ is the surface stress. Field measurements have been conducted by Snyder and Cox (1966), Barnett and Wilkerson (1967), Dobson (1971), Elliott (1972), Snyder (1974), and Snyder, Long, Dobson, and Elliott (1977).

Snyder and Cox (1966) measured the wave growth by employing an array of wave recorders towed at the wave group velocity. Barnett and Wilkerson (1967) measured the wave growth by an aircraft-mounted radar altimeter. They both found the values of β derived from the wave growth rate to be one order of magnitude larger than Miles' theoretical values. However, wave growth rates are determined by the combined effects of wind generation and nonlinear wave energy transfer. Their β values contain both wind generation and nonlinear energy transfer contributions to the forward face of the wave spectrum (See Chapter II, B).

Dobson (1971) measured the atmospheric pressure above waves by using a buoy-mounted pressure sensor. The resulting energy input by wind was one order of magnitude greater than that predicted by Miles. Elliott (1972) measured the atmospheric pressure above waves by using a vertical array of fixed pressure sensors. The energy input was approximately double that of Miles'. Snyder (1974) measured the atmospheric pressure above waves by using probes at fixed elevations. His results were comparable with Miles'. The joint experiment held in the Bight of Abaco, Bahamas, by Snyder, Long, Dobson and Elliott (1977) included instrumentation systems provided by Dobson, Elliott and

Snyder. The simultaneous use of those instruments helped to resolve some of the differences between previous independent field measurements. Dobson and Elliott (1977) found, from data obtained by Elliott's pressure instruments, that

$$\beta = 0.25 \left(\frac{U_5}{c} \cos \theta_w - 1 \right) , \qquad (2\text{-}8)$$

where U_5 is the wind velocity at 5 m above the mean water surface, c is wave phase velocity, and θ_w is the angle between the wave and the wind directions. Snyder et al. (1977), by using the full data set, found their results very close to those shown above. Their results are as follows

$$\beta = 0.2 \begin{pmatrix} +0.1 \\ -0.05 \end{pmatrix} \left(\frac{U_5}{c} \cos \theta_w - 1 \right) . \qquad (2\text{-}9)$$

A comparison between the various theoretical and experimental values of β is shown in Figure 3.

3. Assessment

Miles' theory was a breakthrough in understanding the energy transfer from wind to waves. The early data (Snyder and Cox, 1966, and Barnett and Wilkerson, 1967) showed the measured wave growth rates to be one order of magnitude greater than Miles' theoretical predictions of the wind input rates. However, it was found later that the wind wave growth is not the result of wind input only. The transfer of energy by nonlinear interaction is also responsible for the wave growth. The field measurements by Elliott (1972), Snyder (1974), and Snyder, Long, Dobson and Elliott (1977) and the theoretical calculations by Townsend (1972) and Gent and Taylor (1976) all suggested the atmospheric transfer rates of the same order of magnitude as Miles' theory.

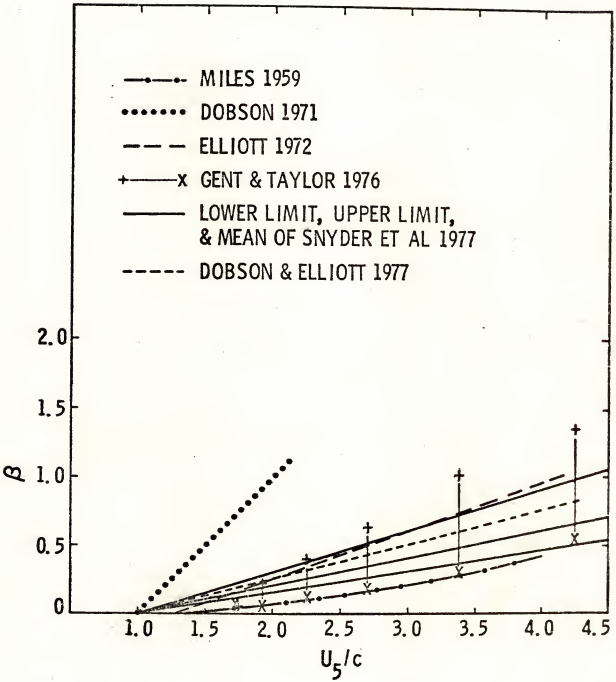

Figure 3. Some theoretical and experimental results on the values of β.

In 1977 Dobson and Elliott recalculated Elliott's 1972 data results, and Snyder et al. corrected Snyder's 1974 results. Comparisons of these results and those of later experiments give average growth rates of about twice those of Miles' theoretical values. The results of Dobson and Elliott (1977), $\beta = 0.25\ (U_5 \cos\theta_w/c - 1)$, are close to this average.

II.B. Nonlinear Wave Energy Transfer

1. Theories

The nonlinear resonant interactions among gravity water waves was first pointed out by Phillips (1960). He carried out the perturbation expansion about the linear wave solution and found that unsteady perturbations were possible at the third order in the expansion under the resonance condition, i.e.,

$$\begin{aligned} \omega_1 + \omega_2 - \omega_3 - \omega_4 &= 0 \quad , \\ \vec{k}_1 + \vec{k}_2 - \vec{k}_3 - \vec{k}_4 &= 0 \quad , \end{aligned} \tag{2-10}$$

where ω's are frequencies and k's are corresponding wave numbers. When Equation (2-10) is satisfied, there is a continuous flow of energy among those four waves.

Following Phillips, the nonlinear interaction theory has been extended by Longuet-Higgins (1962), Longuet-Higgins and Phillips (1962), Benney (1962), and Bretherton (1964) and has been demonstrated in laboratories by Longuet-Higgins and Smith (1966) and McGoldrick, Phillips, Huang, and Hodgson (1966).

The effect of nonlinear wave-wave interaction on the energy transfer among wave components of a wave spectrum was investigated by

Hasselmann (1962, 1963a, 1963b). He used a fifth order perturbation method to obtain an equation which expresses the time-rate change of energy density at wave number $\vec{k}_4$ due to the nonlinear interaction of waves with wave number $\vec{k}_1$, $\vec{k}_2$ and $\vec{k}_3$. His equation reads

$$\frac{\partial F(\vec{k}_4)}{\partial t} = \int \omega_4 \pi \left(\frac{3D_1}{2\rho\omega_1\omega_2\omega_3\omega_4} \right)^2 [\omega_4 F_1 F_2 F_3 + \omega_3 F_1 F_2 F_4 - \omega_2 F_1 F_3 F_4 - \omega_1 F_2 F_3 F_4] \, \delta(\omega_1 + \omega_2 - \omega_3 - \omega_4) \, \delta(\vec{k}_1 + \vec{k}_2 - \vec{k}_3 - \vec{k}_4) \, d\vec{k}_1 \, d\vec{k}_2 \, d\vec{k}_3 \quad , \tag{2-11}$$

where $D_1 = D_1(k_1, k_2, k_3, \omega_1, \omega_2, \omega_3, h)$ is the interaction coefficient and h is the water depth.

The numerical computations of Equation (2-11) for deep water wave spectra have been carried out by Sell and Hasselmann (1972). The computation results were discussed in JONSWAP (Joint North Sea Wave Project) report by Hasselmann et al. (1973). Their computations show that for a white spectrum with a low frequency cutoff, the nonlinear energy transfer tends to enhance the energy level toward the low frequency end of the distribution, forming a peak. The peak keeps growing and narrowing as the spectrum evolves to a Pierson-Moskowitz spectrum (Figure 4). As the peak continues to grow and to narrow (Figure 5), it shifts toward the lower frequency until the spectrum reaches a state where the peak no longer grows but it still shifts toward the lower frequency (Figure 6). Finally, for an extremely narrow spectrum, the nonlinear energy transfer tends to broaden and flatten the peak (Figure 7). The latter provides an explanation for the self-stabilizing property of a wind wave spectrum.

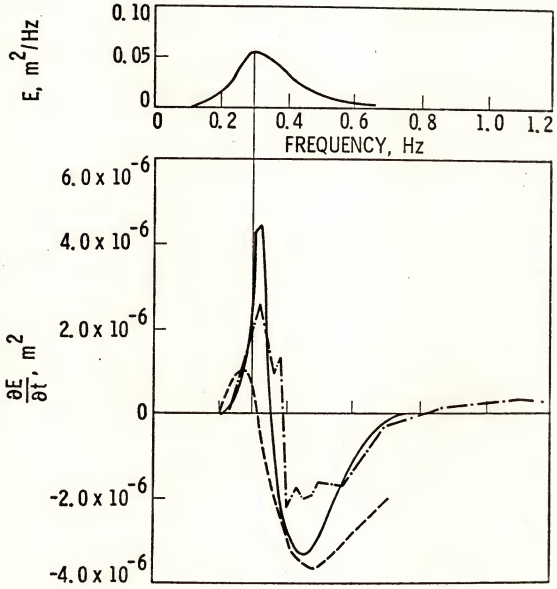

Figure 4. Computed nonlinear energy transfer for a Pierson-Moskowitz spectrum.

a) — · — Sell and Hasselmann (1972)
b) ——— This dissertation
c) ----- Computed by Barnett's (1966) parametric equation.

Figure 5. Computed nonlinear energy transfer for a broad JONSWAP spectrum.

a) — · — Sell and Hasselmann (1972)
b) ——— This dissertation
c) ----- Computed by Barnett's (1966) parametric equation.

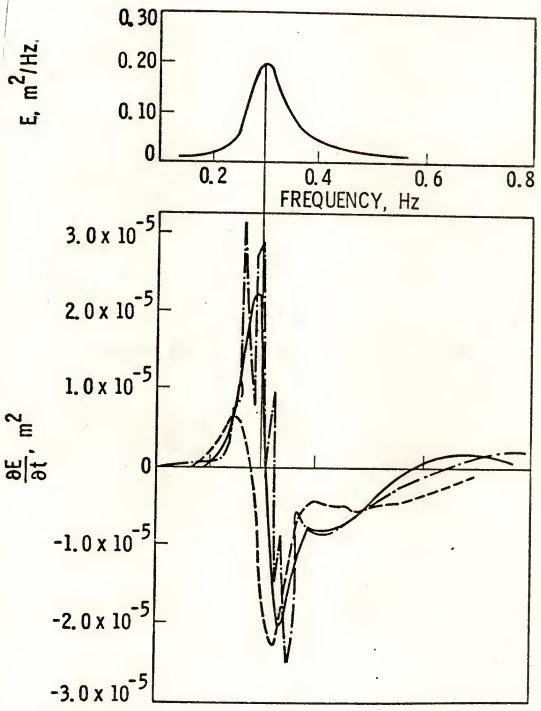
E, m²/Hz
0.30
0.20
0.10
0
0.2
0.4
0.6
0.8
FREQUENCY, Hz
∂E/∂t, m²
3.0 x 10⁻⁵
2.0 x 10⁻⁵
1.0 x 10⁻⁵
0
-1.0 x 10⁻⁵
-2.0 x 10⁻⁵
-3.0 x 10⁻⁵

Figure 6. Computed nonlinear energy transfer for a mean JONSWAP Spectrum.

a) — · — Sell and Hasselmann (1972)
b) ——— This dissertation
c) ----- Computed by Barnett's (1966) parametric equation.

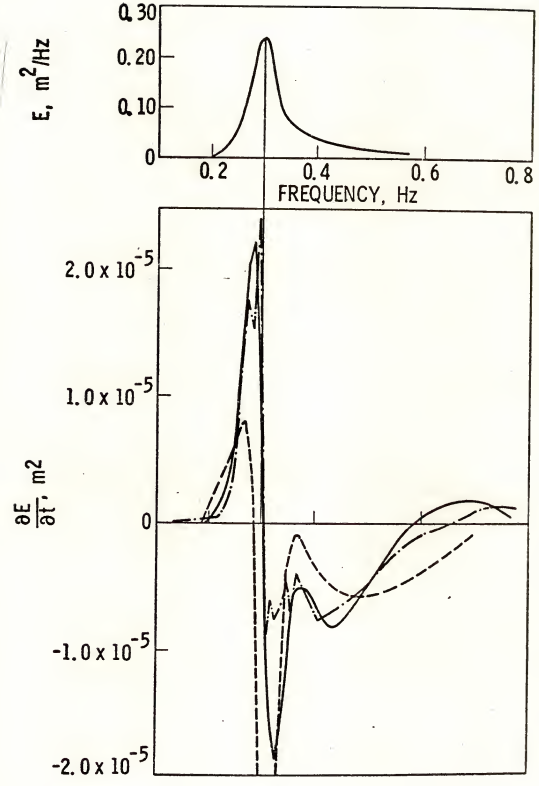
E, m²/Hz
0.30
0.20
0.10
0
0.2
0.4
0.6
0.8
FREQUENCY, Hz
2.0 x 10⁻⁵
1.0 x 10⁻⁵
0
-1.0 x 10⁻⁵
-2.0 x 10⁻⁵
∂E/∂t, m²

Figure 7. Computed nonlinear energy transfer for a sharp JONSWAP Spectrum.

a) — — Sell and Hasselmann (1972)
b) ——— This dissertation
c) ---- Computed by Barnett's (1966) parametric equation.

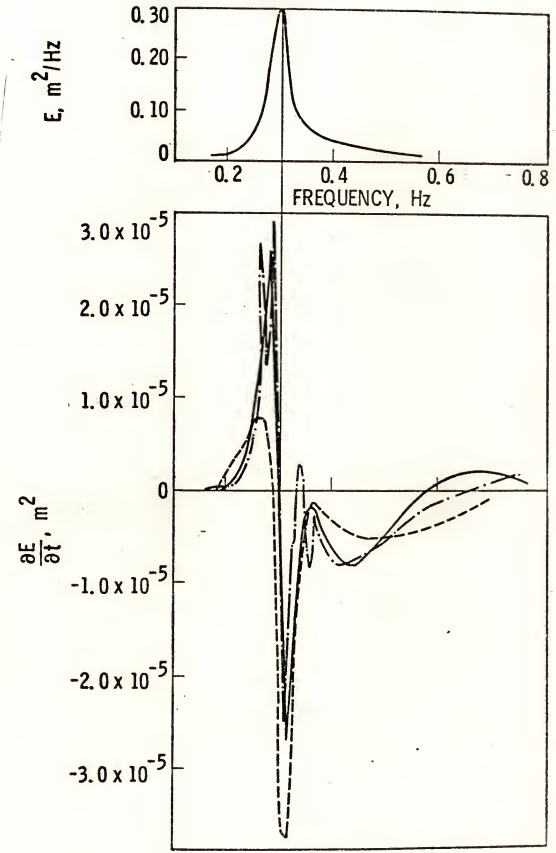
E, m²/Hz
0.30
0.20
0.10
0
0.2
0.4
0.6
0.8
FREQUENCY, Hz
3.0 x 10⁻⁵
2.0 x 10⁻⁵
1.0 x 10⁻⁵
0
-1.0 x 10⁻⁵
-2.0 x 10⁻⁵
-3.0 x 10⁻⁵
∂E/∂t, m²

Hence, the forming of the spectral peak, the rapid growth of the forward face of a spectrum, and the shifting of the peak toward the lower frequency can all be explained by the nonlinear energy transfer.

Longuet-Higgins (1976) assumed a narrow spectrum and developed an equation similar to Equation (2-11) by using the equation for the evolution of wave packets in three dimensions. Fox (1976) calculated the energy transfer in a spectrum based on Longuet-Higgins' equation and obtained results comparable to those of Sell and Hasselmann (1972).

The interaction between short gravity waves and long gravity waves in which the wave length of long waves is much longer than that of short waves is a different mechanism. The oscillatory variations of short waves which are phase related to the long wave profile are induced by the orbital velocity of the long wave. If short waves are steep enough or the orbital velocity of long waves is strong enough, short waves will break near the crest of long waves. Phillips (1963) predicted that breaking can siphon energy from the long waves and thus contribute to their decay. On the other hand, Longuet-Higgins (1969) argued that breaking can transfer energy to the long waves and cause them to grow. Hasselmann (1971), by considering both mass and energy transfers, showed that this kind of interaction always attenuates long waves. The attenuation rate is negligible, however, in both wind wave and swell cases.

2. Experiments

Mitsuyasu (1968) measured the energy transfer in the wind-generated wave spectra in the decay area of a wind-wave tank. The results had the same characteristics as the parameterized nonlinear

energy transfer function modified from Barnett's (1968) parameterized function. An example is shown in Figure 8.

Hasselmann et al. (1973) compared the computed theoretical nonlinear energy transfer functions with the observed source functions for wave spectra measured in the North Sea. Again, they showed good agreements on the shapes. The results tend to confirm the nonlinear wave-wave interaction theory and indicate that nonlinear energy transfer plays a major role in the wave growth process. An example is shown in Figure 9.

3. Assessment

As indicated above, the nonlinear energy transfer mechanism is able to explain the rapid growth of the forward face of a spectrum, the forming of the spectral peak, and the shifting of the peak toward lower frequency. It now appears to be the major mechanism in the development of a spectrum. The energy balance in a wind wave spectrum at 125 nautical miles fetch and 17 m/sec wind speed is shown in Figure 10. It is taken from the computation in Chapter VI, D. It shows how the nonlinear transfer plays the key role in the evolution of a spectrum.

The high growth rates obtained by Snyder and Cox (1966) and Barnett and Wilkerson (1967) can now be explained by the nonlinear energy transfer. The growth rates Snyder and Cox reported were for waves at the forward face of the spectrum. Barnett and Wilkerson's growth rates are for waves with frequencies lower than or near the spectral peak. From the nonlinear energy transfer theory, the growth rate of such waves is mostly due to the contribution of the nonlinear

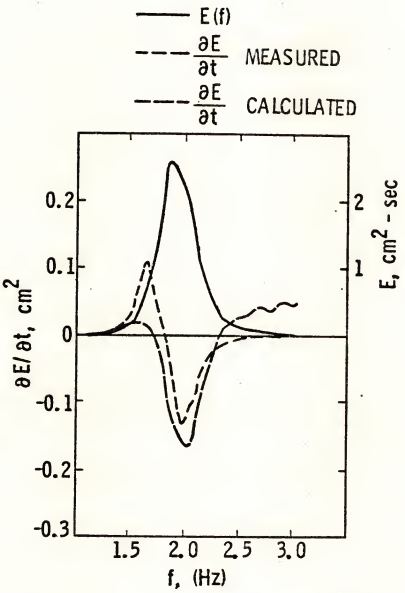

Figure 8. Laboratory wave spectrum and the rate of energy transfer [After Mitsuyasu (1968)].

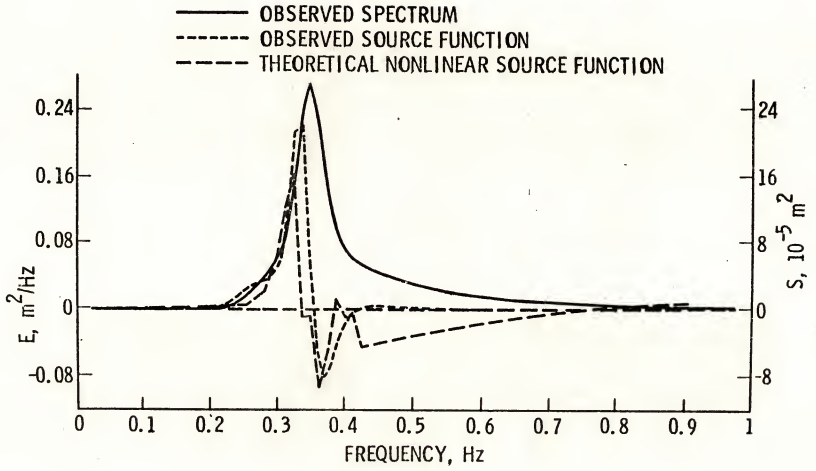

Figure 9. Field wave spectrum and the rate of energy transfer [After Hasselmann et al. (1973)].

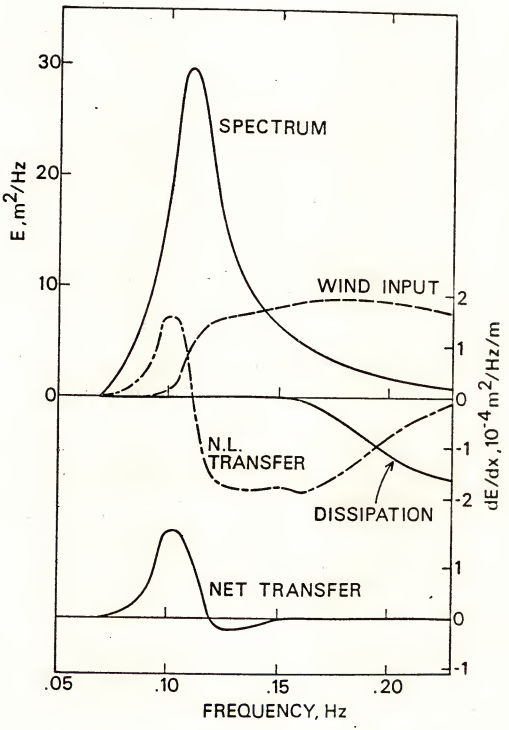

Figure 10. Energy balance in a wind wave spectrum.

transfer rather than the direct wind input. The energy transfer rates from wind to waves were greatly overestimated since they were derived strictly from wave growth data.

CHAPTER III

REVIEW OF WAVE PREDICTION TECHNIQUES

In this Chapter the existing wave prediction models in both deep and shallow water are classified into several groups according to the type of prediction technique. A brief review and an assessment are given for each group of models.

III.A. Deep Water Models

1. Empirical Methods

These methods include the so-called S-M-B method and the P-N-J method. The S-M-B method is the "significant wave method" developed by Sverdrup and Munk (1947) and later revised by Bretschneider (1951, 1958). The significant wave height and significant wave period can be estimated by the empirical relationships between these wave variables and wind speed, duration and fetch. The P-N-J method is the "wave spectrum method" developed by Pierson, Neumann, and James (1955). The wave spectrum can be predicted also by using the empirical relationships between wave characteristics and wind speed, duration, and fetch.

These methods are entirely empirical. There is no consideration of the physical processes involved in wave development such as generation, interaction, etc. Following the advances in wave theories, more sophisticated wave prediction methods have been developed.

2. P-T-B Type Model

This type of model predicts waves by solving the spectral energy balance equation numerically for each frequency and direction component of the spectrum. The P-T-B type model was developed by Pierson, Tick, and Baer (1966). This model type includes those by Inoue (1967), Lazanoff, Stevenson, and Cardone (1973), Salfi (1974), and Cardone, Pierson, and Ward (1976). The energy equation of this type model is in the form of

$$\frac{DE}{Dt} = (A_m + B_m E)\left[1 - \left(\frac{E}{E_\infty}\right)^2\right] \quad , \tag{3-1}$$

where E is the wave spectrum, and E_∞ is the fully developed wave spectrum. The term $[1 - (E/E_\infty)^2]$ is used to limit the spectral growth to E_∞ which implicitly includes the mechanism of wave breaking. A_m and $B_m E$ are similar to Phillips' linear growth term and Miles' exponential growth term respectively. The values of A_m and B_m are determined from wave growth rate measurements. The values of B_m which were used are much higher than Miles' theoretical results. In their equation the important nonlinear energy transfer term is missing. Therefore, their A_m and B_m terms include not only the atmospheric input but also the nonlinear energy transfer. Although wave growth can be predicted the underlying physics is incorrect.

3. B-E Type Model

This type includes models by Barnett (1968) and Ewing (1971). The B-E type model predicts waves by solving a different form of the spectral energy balance equation

$$\frac{DE}{Dx} = (A_m + B_m E)(1 - Q) + (\Gamma - \xi E) \quad , \tag{3-2}$$

where Q is the wave breaking parameter which again limits the wave growth and which implicitly includes the wave breaking mechanism. The term ($\Gamma - \xi E$) is the parameterized representation of the nonlinear energy transfer. Although this type of model includes the nonlinear energy transfer term in the energy balance equation, the values of A_m and B_m are determined from the wave growth measurements which include both atmospheric input and nonlinear energy transfer contributions. Therefore, the atmospheric input is overestimated.

4. Parametric Model

The parametric wave prediction model was developed by Hasselman, Ross, Müller, and Sell (1976). Their model is based on the JONSWAP spectrum (Figure 11) which is in the form of

$$E(f) = \frac{\alpha_e g^2}{(2\pi)^4 f^5} \exp\left[-1.25\left(\frac{f_m}{f}\right)^4\right] \gamma_p \exp\frac{-(f - f_m)^2}{2\sigma^2 f_m^2} , \qquad (3\text{-}3)$$

where $\sigma = \sigma_a$ for $f \leq f_m$, $\sigma = \sigma_b$ for $f > f_m$ and f_m is the peak frequency, α_e is the equilibrium constant, γ_p is the peak enhancement factor, σ_a is the left peak width, and σ_b is the right peak width. They found that the JONSWAP spectrum fits measurements obtained under both stationary fetch-limited wind conditions and growing wind seas. They explain this by the shape-stabilizing influence of the nonlinear resonant wave-wave interaction process which controls the evolution of a spectrum in a growing sea. Their model is formulated by the projection of the energy balance equation

$$\frac{dE}{dt} = S ,$$

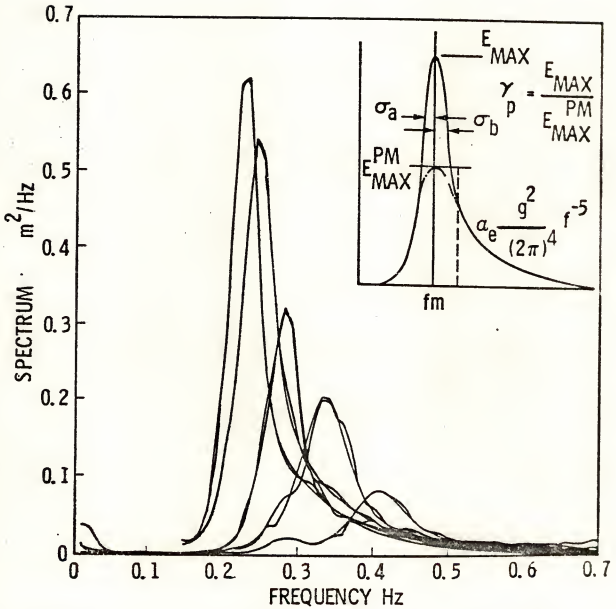

Figure 11. Evolution of wave spectrum with fetch. The best fit JONSWAP Spectra are also shown. The insert illustrates the definition of the five free parameters of a JONSWAP spectrum [After Hasselmann et al. (1973)].

where S is source function, onto a set of parametric transport equations. Assuming constant γ_p, σ_a, and σ_b, the equations for the two-parameter (f_m and α_e) model are

$$\frac{1}{\nu_m}\left(\frac{\partial \nu_m}{\partial q} + P_{\nu\nu}\frac{\partial \nu_m}{\partial \ell}\right) + P_{\nu\alpha}\frac{1}{\alpha_e}\frac{\partial \alpha_e}{\partial \ell} = -N_\nu \alpha_e^2 \nu_m + \frac{1}{U_{10}}\left(\frac{\partial U_{10}}{\partial q} + \frac{\partial U_{10}}{\partial \ell}\right), \qquad (3\text{-}4)$$

$$\frac{1}{\alpha_e}\left(\frac{\partial \alpha_e}{\partial q} + P_{\alpha\alpha}\frac{\partial \alpha_e}{\partial \ell}\right) + P_{\alpha\nu}\frac{1}{\nu_m}\frac{\partial \nu_m}{\partial \ell} = I\,\nu_m^{7/3} - N_\alpha \alpha_e^2 \nu_m + \frac{0.2}{U_{10}}\left(\frac{\partial U_{10}}{\partial \ell}\right) \qquad (3\text{-}5)$$

where

$$\begin{pmatrix} P_{\nu\nu} & P_{\nu\alpha} \\ P_{\alpha\alpha} & P_{\alpha\nu} \end{pmatrix} = \begin{pmatrix} 1 & -0.07 \\ 0.47 & 0.2 \end{pmatrix}, \quad N_\nu = 0.54,\ N_\alpha = 5,\ I = 0.0051 ,$$

and $\nu_m = f_m U_{10}/g$, U_{10} = wind speed at 10 m height, $\partial/\partial q = (U_{10}/g)\,\partial/\partial t$, $\partial/\partial_\ell = (U_{10}/g)\,\vec{V}_m \cdot \nabla$, with $\vec{V}_m$ parallel to the wind direction, and $|\vec{V}_m| = 0.85g/4\pi f_m$. This set of equations is solved numerically by using finite difference techniques. A further simplification is made by assuming a quasi-equilibrium relationship between α_e and ν_m. Thus, only one equation in ν_m is required in the most simple case.

This model predicts waves by solving only one or two parametric transport equations instead of the energy balance equation for each of the wave components. It greatly simplifies the wave prediction technique and the numerical calculations, but there are disadvantages. For instance, it cannot be used conveniently for the prediction of swell or swell and sea combination, or in variable wind field situations. In addition, the wave tranformation mechanisms in shallow water cannot be easily added to this model.

III.B. Finite-Depth Water Models

1. Modified S-M-B Method

In 1954, Bretschneider presented a method for predicting the properties of waves generated in finite-depth water. This model was generated by combining the S-M-B method and the theory of friction and percolation dissipation which had been formulated by Bretschneider and Reid (1954). This method has been revised by Bretschneider (Shore Protection Manual, U.S. Army Coastal Engineering Research Center, 1973) and is still being used. However, this method, like the deep water S-M-B method, is highly empirical.

2. Collins' Model

Collins (1972) developed a finite-depth water wave prediction model which predicts waves by solving the energy balance equation numerically in shallow water. It included the mechanisms of refraction, shoaling, wind generation, bottom friction, and wave breaking. He used Barnett's (1968) generation terms but did not include the nonlinear energy transfer mechanism. He also neglected the energy dissipation by percolation which can be important in a sandy bottom. In his model, the equation for the principal direction of the bottom velocity field [Collins (1972), Eq. (13)] is incorrect. Its correct form reads

$$\cos^4\theta - \cos^2\theta + \frac{\alpha_2^2}{4\alpha_2^2 + (\alpha_3 - \alpha_1)^2} = 0$$

[following Collins' (1972) notations for comparison]. In addition, the Hurricane Betsy wave data which Collins used for verifying his model

are now open to question. The wave height spectra were derived from bottom pressure measurements offshore of Panama City, Florida. A careful reexamination of the data reveals that the spectra at Stage I in Collins' Fig. 10 and Fig. 11 have lower energy levels than those carefully calculated from the same data. The differences appear to be due to errors in the use of conversion factors. The correct spectra require higher energy dissipation rates to match the predicted and measured spectra at Stage II.

3. Monochromatic Wave Model

Skovgarrd, Jonsson, and Bertelsen (1975) presented a method to compute the wave height change for monochromatic waves due to refraction, shoaling, and friction only. The remaining wave transformation mechanisms, such as generation, nonlinear transfer, percolation, etc., were not considered. Therefore, its use is greatly limited.

III.C. Comments

With the possible exception of the parametric model, none of the existing models incorporate the correct physical processes of wave growth. But the use of the parametric model is restricted to deep water and only simple generation conditions can be considered in its present form. The wave prediction in finite-depth water is more complex and consequently only a few models have been proposed to date. Of those none have carefully considered all the important wave transformation mechanisms. The model presented in this dissertation is the first attempt to incorporate all the important transformation mechanisms in finite-depth water and the correct wave growth process.

CHAPTER IV

WAVE TRANSFORMATION MECHANISMS IN FINITE-DEPTH WATER

The wave transformation mechanisms of nonlinear interaction, wave-soft bottom interaction, bottom friction, percolation, wave breaking, and wind generation are discussed in this chapter. The proper expressions for these mechanisms will be chosen from existing theories and available data or independently derived.

IV.A. Nonlinear Energy Transfer

The discussion in Chapter II,B, on nonlinear interaction is for deep water waves only. The effects of nonlinear interaction on the energy transfer for shallow water waves has only recently been studied. Herterich and Hasselmann (1978) assumed a narrow band spectrum to derive a simplified expression for the interaction coefficient [the term D_i in Equation (2-11)] in finite-depth water. They found that the nonlinear transfer in shallow water is one order of magnitude greater than in deep water (Figure 12). The significance of nonlinear energy transfer on the shallow water wave spectrum has been demonstrated by Shemdin, Hasselmann, Hsiao, and Herterich (1977) by using the computation method suggested by Herterich and Hasselmann (1978). This method is also used in this model. The steps in the computation are: (1) redistributing the directional energy distribution so that it is comparable to the deep water spectrum; (2) computing the nonlinear energy transfer by considering the redistributed spectrum as a deep

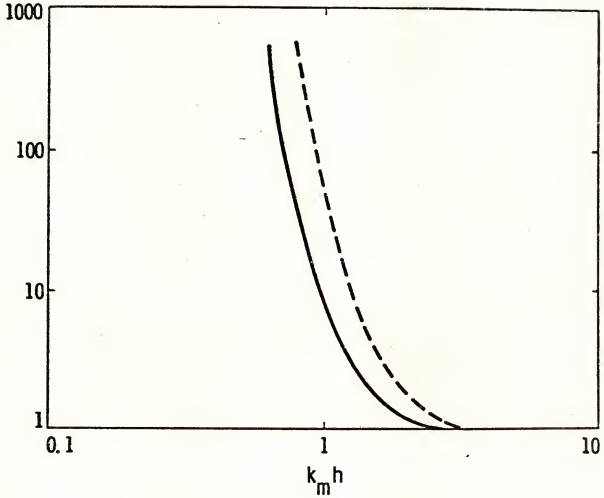

Figure 12. The effective ratio of nonlinear transfer rates in the finite depth water to that in the deep water (——) and the factor, R_t (----), for computing the transfer rate in finite-depth water [after Herterich and Hasselmann (1978)].

water case; (3) multiplying the transfer rate by a factor R_t (Figure 12) which is a function of $k_m h$; (4) transforming the results back to the original directional energy distribution.

For step (2), Equation (2-11) should be used for optimum accuracy. However, this computation is very complicated and time consuming. Typical computation time on a CDC 6600 computer is 30 minutes for one spectrum (Hasselmann et al., 1973). It would be impractical to impose such a computation at every grid point in a prediction model. To evaluate the nonlinear energy transfer rapidly and accurately, Barnett (1968) and Ewing (1971) separately developed parameterized representations for Equation (2-11) based on Hasselmann's (1963b) earlier computation results. In this model, Barnett's parameterized equation is modified on the basis of later improved computations by Sell and Hasselmann (1972). The modified equation is

$$\left(\frac{DE(f,\theta)}{Dt}\right)_{N.L.} = \Gamma - \xi E(f,\theta) \ , \tag{4-1}$$

where

$$\Gamma = 1.10 \times 10^{9} \ E_T^3 \ f_o^{4.5} \ f^{0.5} \ (f - 0.42 f_o)^3 \ \cos^4(\theta - \theta_o)/g^4$$

$$\times \exp\left\{0.693 e^{-100(f/f_o - 0.81)^2} - 1.45 \ |f/f_o - 0.85|^{0.625} - 2.388 \ |f/f_o - 0.8|^{1.5}\right\} \ , \tag{4-2}$$

$$\xi = 1.17 \times 10^{8} \ E_T^2 \ f_o^5 \ f \ [1 + 16 \ |\cos(\theta - \theta_o)|] \ (f - 0.54 \ f_o)^3$$

$$\times \exp\left\{-2.388 \ |f/f_o - 0.8|^{1.5}\right\} \ , \tag{4-3}$$

and

$$E_T = \iint E(f,\theta) \ df \ d\theta ,$$

$$f_o = \frac{1}{E_T} \iint fE(f,\theta)\, df\, d\theta,$$

$$\theta_o = \frac{1}{E_T} \iint \theta E(f,\theta)\, df\, d\theta. \qquad (4\text{-}4)$$

When compared with Barnett's original equation, better results are obtained by using the modified equation. The comparisons between Sell and Hasselmann's computations and the parameterized computations are shown in Figures 4 through 7 in Chapter II.

IV.B. Wave-Soft Bottom Interaction

An unusually large amount of wave energy attenuation in the Mississippi Delta area has been reported by Bea (1974) and Tubman and Suhayda (1976). The attenuation cannot be reasonably explained by the mechanisms of refraction, shoaling, bottom friction, nor percolation. It is believed that the excessive attenuation is due to wave-soft bottom interaction. Gade (1958, 1959) studied the dissipation effects of a non-rigid bottom on shallow water long waves. He first considered the bottom to be a viscous fluid and computed the corresponding wave dissipation rate. He later expanded his analysis to a viscoelastic bottom. His results, however, are restricted to only shallow water waves and cannot be applied to intermediate water waves.

Migniot (1968) presented laboratory measurements which showed the orbital motion of mud due to the action of water waves. It indicated that soft mud has the properties of a liquid. Doyle (1973) studied the effect of water waves on clay soil failure in a laboratory soil-wave tank. The effect of mud motion on the wave energy attentuation was not included in his study. Carpenter, Thompson, and Bryant (1973) studied the viscoelastic properties of marine sediments and found a rather

complicated shear stress-shear strain relationship which would be very difficult to apply analytically. Wave height, pressure, current, and bottom movement in East Bay, Louisiana, were measured by Suhayda et al. (1976). Their results indicated close relationships between bottom movements and surface waves. Tubman and Suhayda (1976) found from the field measurements of Suhayda et al. (1976) that the wave energy loss due to mud bottom was at least an order of magnitude greater than that due to percolation or friction. Mallard and Dalrymple (1977) studied the effects of an elastic bottom on water waves. Their results show no wave energy loss because they neglected the viscous property of mud. From field measurements, Rosenthal (1978) studied the wave decay due to the movement of a sandy bottom, and found that this was not a significant effect.

In this dissertation, the wave properties are studied by considering the muddy bottom as a "Voigt body" (Kolsky, 1963). The boundary value problem of water-mud system is solved for sinusoidal waves, then the rate of wave energy dissipation is found from the dispersion equation.

The stress-strain relationship for a Voigt body is

$$\tau = G\varepsilon + \mu\dot{\varepsilon} \quad , \tag{4-5}$$

where τ is shear stress, G is the shear modulus, ρ_m is density, μ is viscosity, ε is shear strain, and $\dot{\varepsilon}$ is the time rate of shear strain. Neglecting the nonlinear terms and assuming constant G, ρ_m, and μ, the two-dimensional equations of motion for a Voigt body become

$$u_{tt} = J \nabla^2 u + \nu \nabla^2 u_t - \frac{1}{\rho_m} p_{xt} \quad , \tag{4-6}$$

and

$$w_{tt} = J \nabla^2 w + \nu \nabla^2 w_t - \frac{1}{\rho_m} P_{zt} \quad , \tag{4-7}$$

where the subscripts represent a partial derivative and $J = G/\rho_m$. Eliminating P from Equation (4-6) and Equation (4-7), it follows that

$$u_{ttz} - w_{ttx} = J\,(u_{xxz} + u_{zzz} - w_{xxx} - w_{xzz}) + \nu(u_{xxzt} + u_{zzzt} - w_{xxxt} - w_{xzzt}). \tag{4-8}$$

To get a periodic solution an oscillatory stream function

$$\psi = s(z)\, e^{i(kx - \omega t)} \quad , \tag{4-9}$$

is assumed and substituted into Equation (4-8). The stream function, ψ, is defined such that $u = \psi_z$ and $w = -\psi_x$. From a partial differential equation, by introducing the stream function, an ordinary differential equation is obtained

$$s_{zzzz} + \left(-2k^2 + \frac{\omega^2}{J - i\nu\omega}\right) s_{zz} + \left(k^4 - \frac{\omega^2 k^2}{J - i\nu\omega}\right) s = 0. \tag{4-10}$$

The solution of Equation (4-10) is

$$s = Ae^{kz} + Be^{-kz} + Ce^{mz} + De^{-mz} \quad , \tag{4-11}$$

where

$$m = k\sqrt{1 - \frac{\omega^2}{k^2(J - i\omega\nu)}} \quad , \tag{4-12}$$

and A, B, C, and D are constants and will be determined from the solution of the water layer equation and the boundary conditions.

The governing equation in the water layer is

$$\nabla^2 \phi = 0 \quad , \tag{4-13}$$

where ϕ is the potential function, i.e., $u = \phi_x$, $w = \phi_z$.

The boundary conditions are (see Figure 13)

$$P = 0 \qquad \text{at } z = h ,$$

$$w = \frac{\partial \eta}{\partial t} \qquad \text{at } z = h ,$$

$$(P)_{water} = (P)_{mud} \qquad \text{at } z = 0 ,$$

$$\left(\frac{\partial u}{\partial z} + \frac{\partial w}{\partial x}\right)_{mud} = 0 \qquad \text{at } z = 0 ,$$

$$(w)_{water} = (w)_{mud} \qquad \text{at } z = 0 ,$$

$$u = 0 \qquad \text{at } z = -H ,$$

$$w = 0 \qquad \text{at } z = -H , \qquad (4\text{-}14)$$

where $\eta = ae^{i(kx-\omega t)}$ is the water surface displacement and a is the amplitude of the water wave.

From Equations (4-11), (4-13), and (4-14), it is found that

$$\phi = -\frac{iag}{\omega}\left[\cosh k(z - h) + \frac{\omega^2}{gk}\sinh k(z - h)\right] e^{i(kx-\omega t)} , \qquad (4\text{-}15)$$

and

$$A = \frac{\lambda}{2\Lambda}\left[(k^2 + m^2)\, e^{kH}\cosh mH - \frac{k}{m}(k^2 + m^2)\, e^{kH}\sinh mH - 2k^2\right] ,$$

$$B = \frac{-\lambda}{2\Lambda}\left[(k^2 + m^2)\, e^{-kH}\cosh mH + \frac{k}{m}(k^2 + m^2)\, e^{-kH}\sinh mH - 2k^2\right] ,$$

$$C = \frac{\lambda}{2\Lambda}\frac{k}{m}\left[k^2 e^{mH}\cosh kH - km\, e^{mH}\sinh kH - (k^2 + m^2)\right] ,$$

$$D = \frac{-\lambda}{2\Lambda}\frac{k}{m}\left[k^2 e^{-mH}\cosh kH + km\, e^{-mH}\sinh kH - (k^2 + m^2)\right] , \qquad (4\text{-}16)$$

where

$$\Lambda = (k^2 + m^2)\cosh kH\cosh mH - \frac{k}{m}(k^2 + m^2)\sinh kH\sinh mH - 2k^2 ,$$

$$\lambda = r\frac{ag}{\omega}\left(\cosh kH - \frac{\omega^2}{gk}\sinh kH\right) ,$$

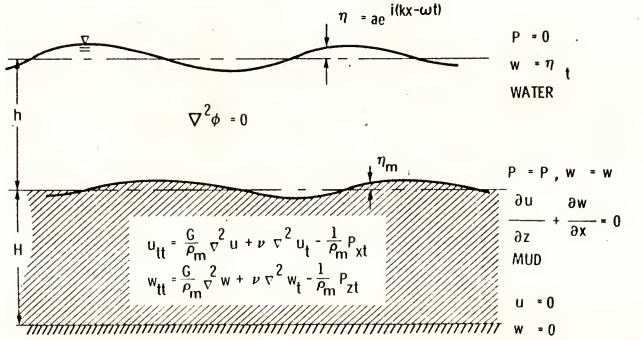

Figure 13. Schematic definition of bottom motion boundary value problem.

r is the ratio of water density to mud density and

$$k = \frac{\omega^2}{g} \frac{1 + \tanh kh \cdot \Omega}{\tanh kh + \Omega} , \qquad (4\text{-}17)$$

where

$$\Omega = r \frac{1}{\lambda} (A + B + C + D) ,$$

or

$$\Omega = r \frac{(m^2 - k^2)(\sinh kH \cosh mH - \frac{k}{m} \cosh kH \sinh mH)}{(m^2 + k^2)(\cosh kH \cosh mH - \frac{k}{m} \sinh kH \sinh mH) - 2k^2} . \qquad (4\text{-}18)$$

Equation (4-17) is the dispersion equation which reduces to the rigid bottom dispersion equation, $\omega^2 = g\, k \tanh kh$, if either there is no mud layer ($H = 0$), the mud layer becomes rigid ($G \to \infty$ or $\nu \to \infty$), or the mud becomes much denser than the water ($r \to 0$).

The wave number k here is a complex number, i.e., $k = k_r + ik_i$. The amplitude of the wave can be written in the form of

$$a(x) = a(x = 0)\, e^{-k_i x},$$

so k_i is a measure of energy dissipation and the dissipation is exponential with distance. The wave number, k, is a function of J, ν, ω, H, and h. The amplitude of a mud wave, η_m, is

$$\eta_m = \eta \left(\cosh kh - \frac{gk}{\omega^2} \sinh kh\right). \qquad (4\text{-}19)$$

The dynamic pressure at the mud line is

$$P = P_f \cosh k_o h \left(\cosh kh - \frac{\omega^2}{gk} \sinh kh\right), \qquad (4\text{-}20)$$

where P_f is the bottom wave dynamic pressure for a firm bottom,

$$P_f = \rho g \eta / \cosh k_o h,$$

and k_o is the wave number for a firm bottom calculated from $\omega^2 = g\, k_o \tanh k_o h$. If the mud layer is very thick ($kH \gg 1$), then Equation (4-18) becomes

$$\Omega = r\, \frac{\omega^2}{2k^2(i\nu\omega - J) + \omega^2} . \qquad (4\text{-}21)$$

Some results of these computations are shown in Figures 14 to 17. The upper Figures show the ratio of the real part of the wave number, k_r, to the wave number of a firm bottom, k_o, as a function of $k_\infty h$ where $k_\infty = \omega^2/g$ is the wave number in deep water. In the lower Figures the ratio of the imaginary part of the wave number, k_i, to k_o is shown.

It can be seen from the upper Figures that k_r approaches k_o when the water is deep; and the larger the values of $J/\omega^2 h^2$ or $\nu/\omega h^2$ are the faster k_r approaches k_o. In the lower Figures k_i/k_o values are shown. They indicate the relative magnitude of wave height attenuation and their values decrease with increasing $k_\infty h$.

In Figures 14 to 16, k_i increases as $J/\omega^2 h^2$ decreases, i.e., the wave attenuation rate is smaller for a more rigid bottom. In Figure 17, k_i increases first then decreases as $\nu/\omega h^2$ increases. This is attributed to the fact that the energy dissipation is proportional to the magnitude of viscosity but the mud movement is smaller when it becomes more viscous. Eventually, the bottom becomes firm when $\nu/\omega h_2 \to \infty$ and there is no energy dissipation by this mechanism.

IV.C. Bottom Friction

Wave energy dissipation due to bottom friction is considered to be the work done against the bottom turbulent shear stresses by the

Figure 14. Real and imaginary parts of wave number. $H/h = 1.0$, $\nu/\omega h^2 = 0.003$. Numbers on the curves refer to $J/\omega^2 h^2$.

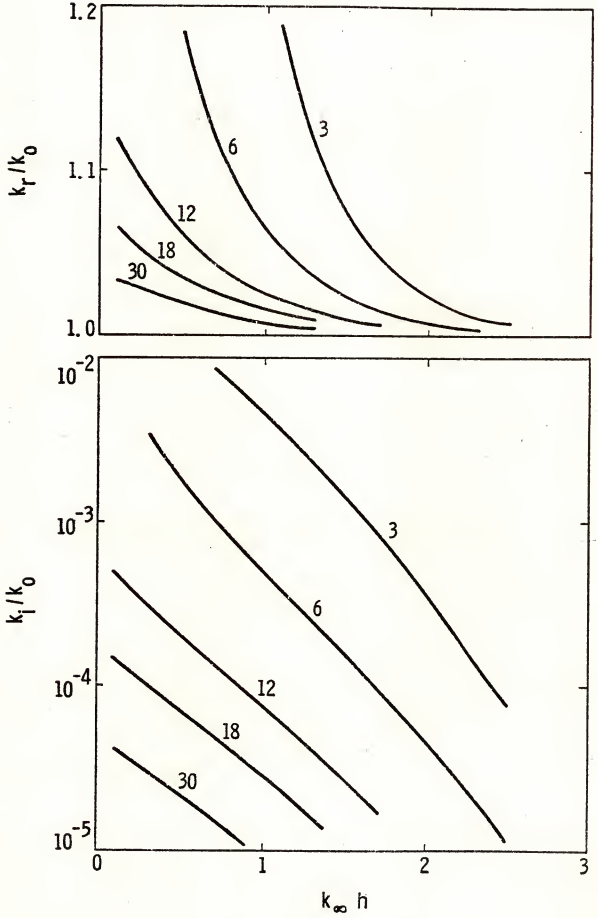
1.2
1.1
1.0
k_r/k_0
3
6
12
18
30
10^{-2}
10^{-3}
10^{-4}
10^{-5}
k_i/k_0
0
1
2
3
$k_\infty h$

Figure 15. Real and imaginary parts of wave number. $H/h = 3.16$, $\nu/\omega h^2 = 0.003$. Numbers on the curves refer to $J/\omega^2 h^2$.

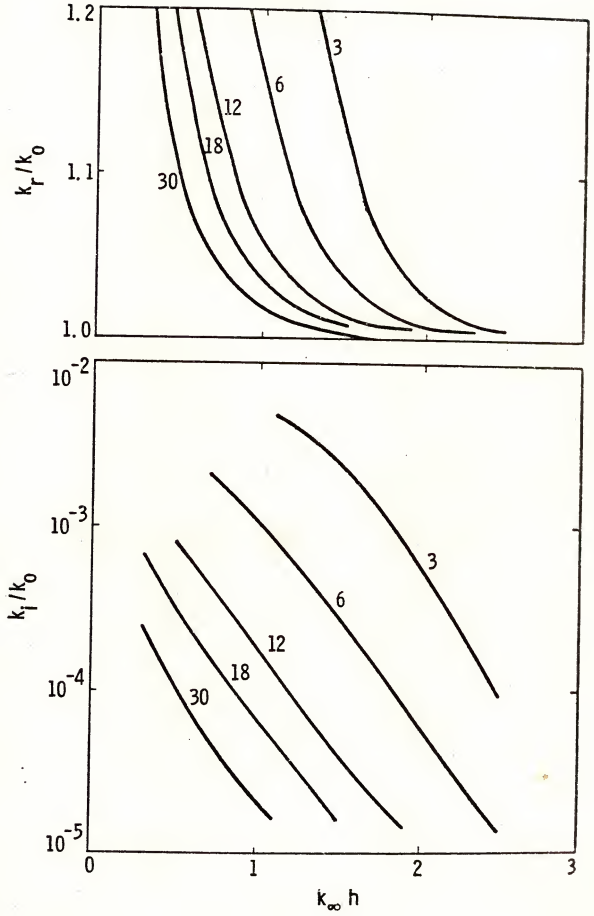
1.2
1.1
1.0
k_r/k_0
3
6
12
18
30
10^{-2}
10^{-3}
10^{-4}
10^{-5}
k_i/k_0
3
6
12
18
30
0
1
2
3
$k_\infty h$

Figure 16. Real and imaginary parts of wave number. $H/h \to \infty$, $\nu/\omega h^2 = 0.003$. Numbers on the curves refer to $J/\omega^2 h^2$.

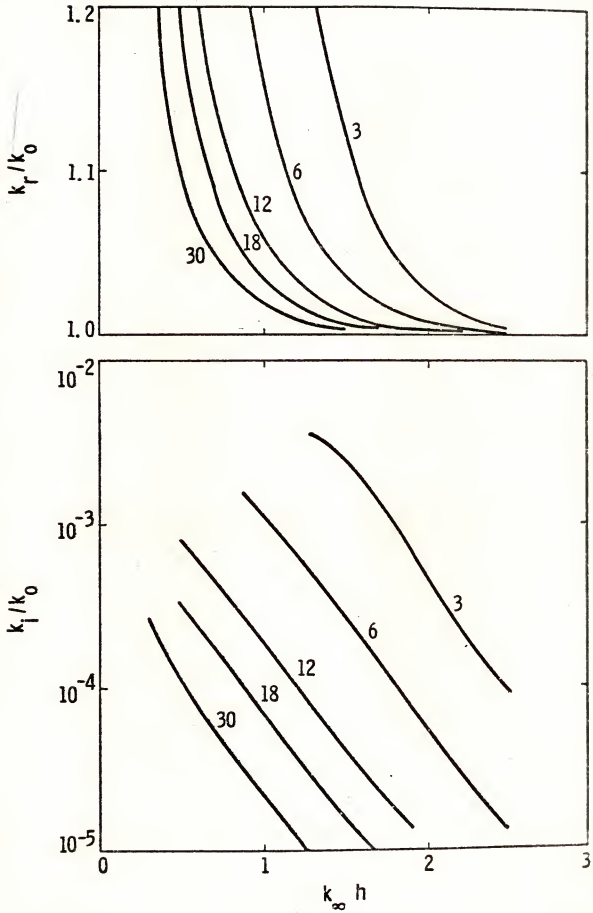
1.2
1.1
1.0
k_r/k_0
3
6
12
18
30
10^{-2}
10^{-3}
10^{-4}
10^{-5}
k_i/k_0
0
1
2
3
$k_\infty h$

Figure 17. Real and imaginary parts of wave number. $H/h \to \infty$, $J/\omega^2 h^2 = 6$. Numbers on the curves refer to $\nu/\omega h^2$.

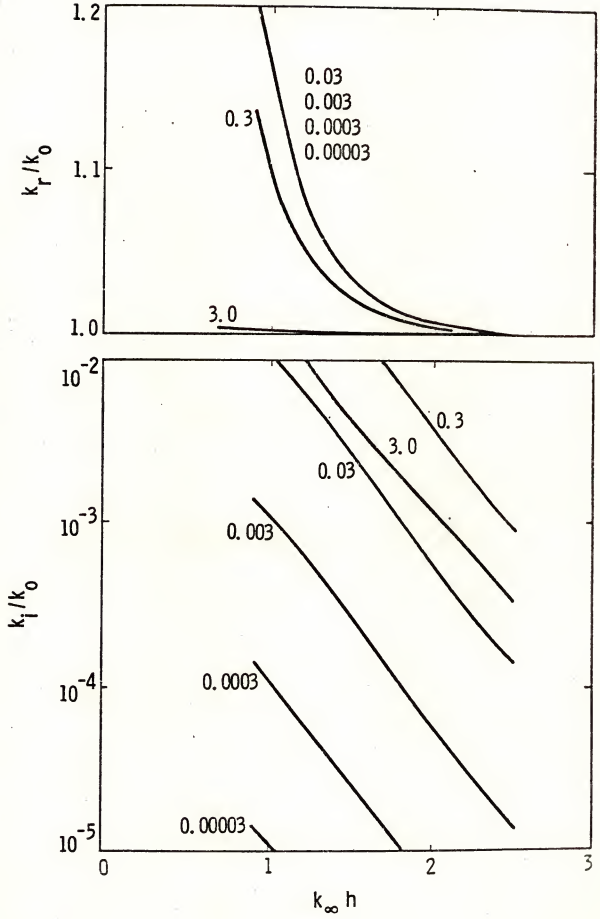
1.2
1.1
1.0
k_r/k_0
0.03
0.003
0.0003
0.00003
0.3
3.0
10^{-2}
10^{-3}
10^{-4}
10^{-5}
k_i/k_0
0.3
3.0
0.03
0.003
0.0003
0.00003
0
1
2
3
$k_\infty h$

wave orbital velocities. The turbulent bottom shear stress can be expressed by the widely accepted quadratic friction law

$$\vec{\tau} = \rho C_f |\vec{W}| \vec{W} \quad , \tag{4-22}$$

where $\vec{\tau}$ is the bottom shear stress, $\vec{W}$ is the velocity just outside the bottom boundary layer, C_f is the friction coefficient, and ρ is the density of water. The friction loss of wave energy has been studied by using the quadratic friction law and assuming monochromatic waves (or using the significant wave height and the significant wave period to represent the entire spectrum) as found in the studies by Putnam and Johnson (1949) and Bretschneider and Reid (1954). Hasselmann and Collins (1968) derived an equation to evaluate the frictional dissipation rate in a wave spectrum by applying the quadratic friction law and the Gaussian properties of the wave field. They found the change in wave energy density at wave number $\vec{k}$ due to friction dissipation to be

$$\frac{DF(\vec{k})}{Dt} = \nu_{ij} \, k_i \, k_j \, F(\vec{k}) \quad , \tag{4-23}$$

which is a linear equation explicitly, but the coefficient ν_{ij} is a function of the entire spectrum as follows

$$\nu_{ij} = \frac{g C_f}{\omega^2 \cosh^2 kh} \left[\delta_{ij} \left\langle |\vec{W}| \right\rangle + \left\langle \frac{W_i \, W_j}{|\vec{W}|} \right\rangle \right] , \tag{4-24}$$

where h is the depth of water and $\langle \; \rangle$ denotes the ensemble average. If the non-wave-induced current is negligible, the ensemble average terms become

$$\left\langle |\vec{W}| \right\rangle = \alpha_f \, E_e \, ,$$

$$\left\langle \frac{W_1^2}{|\vec{W}|} \right\rangle = \alpha_f \left[\frac{E_e}{\gamma_f^2} - \frac{K}{\gamma_f^2} (1 - \gamma_f^2) \right] ,$$

$$\left\langle \frac{W_2^2}{|\vec{W}|} \right\rangle = \alpha_f \frac{1 - \gamma_f^2}{\gamma_f} (K - E_e) \quad , \tag{4-25}$$

where

$$\alpha_f = (2 \langle W_1^2 \rangle / \pi)^{1/2} \quad ,$$

$$\gamma_f = (1 - \langle W_2^2 \rangle / \langle W_1^2 \rangle) \quad ,$$

and

$$K = K(\gamma_f) \quad ,$$

$$E_e = E_e(\gamma_f) \quad ,$$

are complete elliptic integrals of the first and second kind respectively. The coordinate system is chosen such that

$$\langle W_1 W_2 \rangle = 0 \quad , \qquad \text{and} \qquad \langle W_2^2 \rangle < \langle W_1^2 \rangle .$$

The detail of derivation can be found in the Appendix.

In general, the friction coefficient C_f is a function of the wave field and the bottom conditions, but it is regarded as constant for each individual field study. Bretschneider and Reid (1954) found $C_f = 0.01$ based on the wave data obtained offshore of the Louisiana and Texas coast in the Gulf of Mexico. Hasselmann and Collins (1968) found $C_f = 0.015$ for the wave data from offshore of Panama City, Florida, in the Gulf of Mexico. Hasselmann et al. (1973) found $C_f = 0.015$ for swells in the North Sea area. In their study the current modulation of the decay rates predicted by theory was not found (see Figure 18). It led to some uncertainty regarding the applicability of a current dependent friction theory in North Sea area. Alternate mechanisms such as percolation was suggested (Shemdin et al., 1977). Van Ieperen (1975) found $C_f = 0.06 - 0.10$ in his study near Melkbosstrand, South

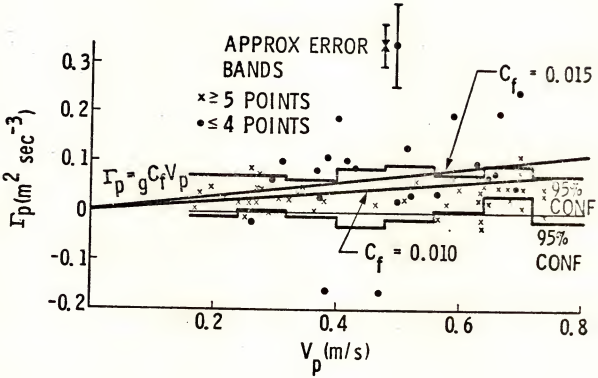

Figure 18. Decay parameter Γ_p vs. current parameter V_p [After Hasselmann et al. (1973)].

Africa. The laboratory study by Jonsson (1965) shows that C_f is a function of the Reynolds number, $R_n = a_m w_m/\nu$, and the relative roughness a_m/k_s, where w_m is the maximum wave orbital velocity just outside the bottom boundary layer, a_m is one-half of the horizontal excursion of a water particle at the edge of the bottom boundary layer, ν is the kinematic viscosity of water, and k_s is the bottom roughness. A friction factor diagram showing the relationships between the friction coefficient, the Reynolds number, and the relative roughness was presented by Jonsson (1965) based on very little data. Expanding the data base through a series of laboratory tests, Kamphuis (1975) presented his friction factor diagram (Figure 19) which will be used in this model.

In order to determine C_f from the wave friction factor diagram, the bottom roughness, k_s, is needed. When the bottom is flat, i.e., no bed forms, the bottom roughness, k_s, is considered to be related to D_n, where D_n is the grain diameter such that n% of the grain size distribution is smaller than D_n. However, the wave orbital flow near the bottom generates sand ripples under certain conditions. The bottom roughness then becomes larger and vortices are generated by the presence of the ripples. Consequently, more wave energy is dissipated. Dingler (1975) conducted laboratory and field experiments and developed the following condition for the onset of grain motion under wave action

$$\frac{\gamma_s T^2}{\rho D_s} = 240 \left(\frac{d_o}{D_s}\right)^{4/3} \left(\frac{\rho \gamma_s D_s^3}{\mu^2}\right)^{-1/9} ,$$

where $\gamma_s = (\rho_s - \rho)\, g$, ρ_s is the density of sand, ρ is the density of water, T is wave period, d_o is the horizontal excursion, D_s is the mean

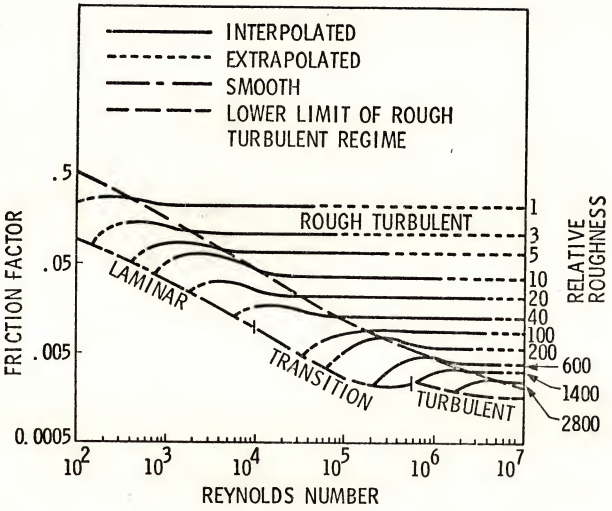

Figure 19. Wave friction factor diagram [After Kamphuis (1975)].

sand diameter, and μ is the viscosity of water. He found that the ripple height and length increased but the ratio of ripple height to ripple length remained constant ($\sim$0.15) as the nondimensional parameter $\theta_s = \rho w_m^2/\gamma_s D_s$ increased up to $\theta_s = 40$. From $\theta_s = 40$ to $\theta_s = 240$, he found that the ripple height-length ratio decreased from 0.15 to 0. For $\theta_s > 240$ the ripples were completely destroyed by the strong wave orbital currents (see Figure 20). In the latter situation the bottom became flat and a sheet flow of sand was formed.

From Figure 20 the ratio of ripple height to length can be determined. The ripple length can be estimated empirically from Figure 21. It depends on the horizontal excursion as demonstrated on the basis of several data sets taken from Dingler (1975). Through these data points, two straight lines are drawn. However, it is likely that more parameters are needed to explain the data scatter. From Figures 20 and 21, one can estimate the ripple height, ζ. Then the roughness height, k_s, can be computed as 4ζ following Jonsson's (1966) suggestion. Finally, C_f can be found from the friction factor diagram shown in Figure 19. The above procedure represents the state of knowledge in determining the friction coefficient at present time. It demonstrates the importance of the knowledge on the interactions between waves and the sand bottom.

There remain other concerns in applying the friction factor diagram for the determination of the friction factor. The grain size distribution of bottom sediments is not always obtained; the relationship between k_s and the ripple height needs to be confirmed; and in cases where the spectrum is not too narrow, the definitions of a_m and w_m need to be specified in spectral terms.

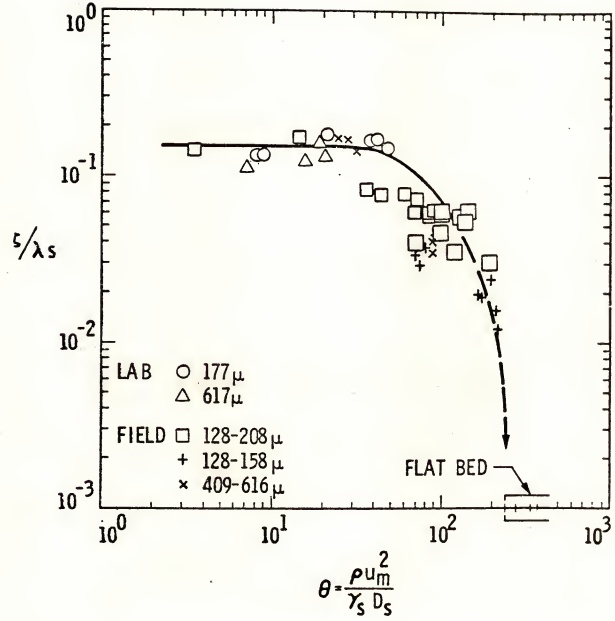

Figure 20. Ripple height-length ratio vs. nondimensional relative stress [after Dingler (1975)].

Figure 21. Relative ripple wavelength vs. relative excursion [data taken from Dingler (1975)].

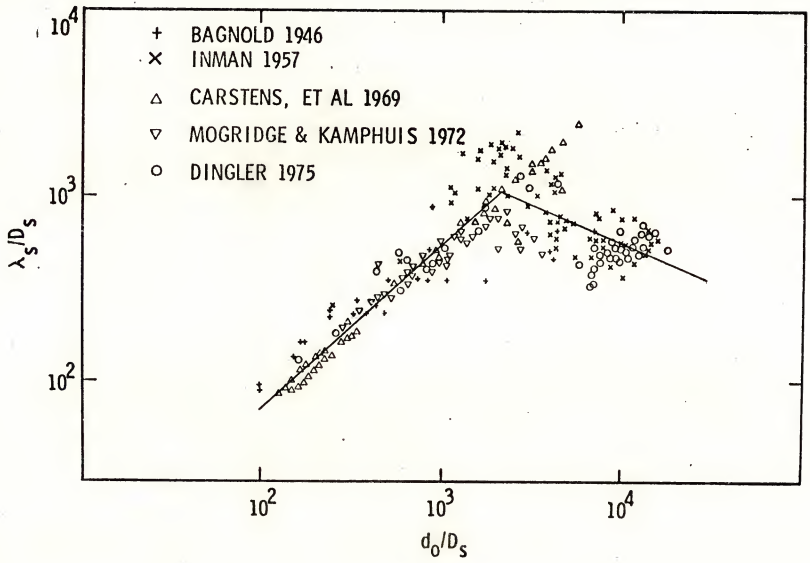
BAGNOLD 1946
INMAN 1957
CARSTENS, ET AL 1969
MOGRIDGE & KAMPHUIS 1972
DINGLER 1975
10^4
10^3
10^2
λ_s/D_s
10^2
10^3
10^4
d_0/D_s

IV.D. Percolation

As waves propagate over a permeable bottom in shallow water, the oscillatory pressure distribution at the bottom forces water through the bottom sand periodically. Wave energy is dissipated by the viscous damping as water flows through the bottom sand. Putnam (1949) was the first to estimate the wave energy dissipation due to percolation in an isotropic permeable bottom sand. However, his calculations overestimate the dissipation rate by a factor of four. Later, Bretschneider and Reid (1954) used Putnam's equation to study wave height modification and consequently overestimated the effect of percolation. A more general equation is derived below.

Darcy's law for flow through a porous medium states

$$u = \frac{k_x}{\rho g}\frac{\partial p}{\partial x} \quad ,$$

$$w = \frac{k_z}{\rho g}\frac{\partial p}{\partial z} \quad , \tag{4-26}$$

where u and w are horizontal and vertical velocities respectively, p is pressure, and k_x and k_z are horizontal and vertical coefficients of permeability respectively. From the conservation of mass,

$$\frac{\partial u}{\partial x} + \frac{\partial w}{\partial z} = o \quad , \tag{4-27}$$

Equation (4-26) becomes

$$\frac{\partial^2 p}{\partial x^2} + \frac{k_z}{k_x}\frac{\partial^2 p}{\partial^2 z} = o \quad . \tag{4-28}$$

The boundary conditions are

$$w = o \text{ at } z = -d \quad ,$$

and

$$p = \rho g n/\cosh kh \text{ at } z = o \quad , \tag{4-29}$$

where η is the displacement of the water surface and d is the thickness of the permeable layer (see Figure 22). The boundary condition for pressure is taken from the linear wave theory for a non-permeable bottom. It is used here because the modification of the wave field by a permeable bottom is at least two orders of magnitude smaller than the wave field of a non-permeable bottom. The solution of Equation (4-28) with boundary conditions (4-29) is

$$p = \rho g \eta \cosh\left[\sqrt{\frac{k_x}{k_z}}\, k(z + d)\right] \Big/ \left[\cosh kh \cosh\left(\sqrt{\frac{k_x}{k_z}}\, kd\right)\right]. \qquad (4\text{-}30)$$

The rate of energy transfer per unit surface area from water to a permeable layer is

$$(pw)_{z=o} = \left(-\frac{k_z p}{\rho g}\frac{\partial p}{\partial z}\right)_{z=o} . \qquad (4\text{-}31)$$

Taking the average over one wave length, Equation (4-31) becomes

$$\frac{DE_m}{Dt} = -E_m k \sqrt{k_x k_z}\, \tanh\left(\sqrt{\frac{k_x}{k_z}}\, kd\right) / \cosh^2 kh \quad , \qquad (4\text{-}32)$$

where $E_m = 1/2\ \rho g a^2$ and a is the amplitude of the wave. For $k_x = k_z$ Equation (4-32) is equivalent to Putnam's (1949) Eq. (19) except for a factor of 4.

From Equation (4-32), the rate of energy dissipation is directly related to the coefficients of permeability. The magnitudes of these coefficients, in turn, depend upon the size and shape of the bottom material. Sleath (1970) found $k_x = 1.3$ cm/sec, $k_z = 0.89$ cm/sec for sand with a median diameter of 1.13 mm and a standard deviation of 0.46 mm; and $k_x = 0.15$ cm/sec, $k_z = 0.13$ cm/sec for sand with a median diameter of 0.388 mm and a standard deviation of 0.101 mm.

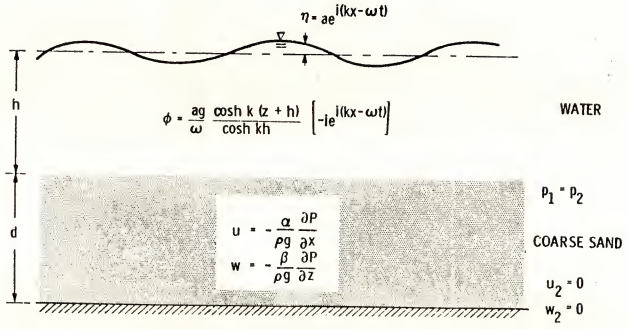

Figure 22. Schematic definition of percolation boundary value problem.

IV.E. Wave Breaking (White Capping)

The growth of wind-generated waves is ultimately limited by their instability which causes their breaking. This breaking process is difficult to measure and, due to its nonlinearity, is difficult to analyze theoretically. In order to consider its effects in a wave model, a limit must be set on the wave spectrum. This limiting spectrum is called the "equilibrium spectrum," and any wave component with an energy density which is higher than this spectrum will eventually modify its energy density by breaking and thereby conforming to the confines of the spectrum.

Phillips (1958) found the equilibrium range of a gravity wave spectrum by using a similarity consideration,

$$\phi_e(f) = \frac{1.17 \times 10^2 \, g^2}{(2\pi)^4 \, f^5} \quad , \tag{4-33}$$

where ϕ_e is the energy density. The numerical constant was found by taking the average of several measurements. Equation (4-33) is valid for frequencies greater than the spectral peak frequency.

The "fully developed spectrum" which is the equilibrium range of the entire spectrum has been proposed in different forms by Neumann (1953), Darbyshire (1955, 1959), Roll and Fischer (1956), Burling (1959), Bretschneider (1959), Pierson and Moskowitz (1964), and Scott (1965). The most widely used spectrum is the Pierson and Moskowitz spectrum

$$E(f) = \frac{\alpha_e \, g^2}{(2\pi)^4 \, f^5} \exp\left[-0.74 \left(\frac{f_w}{f}\right)^4\right] \quad , \tag{4-34}$$

where $f_w = g/2\pi U_{19.5}$, $U_{19.5}$ is the mean wind speed measured at 19.5 m above the sea surface, and $\alpha_e = 0.0081$, is a constant.

Later, Mitsuyasu (1968) and Hasselmann et al. (1973) found that α_e is a function of wind speed and fetch rather than a constant. Hasselmann et al. (1973) also found that the wave energy density near the spectral peak can be much higher than the equilibrium level. Therefore in this model a limiting spectrum in the form of a Pierson and Moskowitz spectrum with a variable α_e (Hasselmann et al., 1973)

$$\alpha_e = 0.076 \left(\frac{F_x g}{U_{10}^2}\right)^{-0.22} ,$$

is used, where F_x is fetch. In order to allow for the spectral peak to grow above the equilibrium level (overshoot), only the portion of the spectrum where $f \geq 1.35\ f_m$ is limited by the equilibrium constraint.

Hasselmann (1974) treated white capping in terms of an equivalent ensemble of random pressure pulses. He showed that

$$\left(\frac{DF(\vec{k})}{Dt}\right)_{\text{breaking}} = \eta_b\, \omega^2\, F(\vec{k}) ,$$

where η_b is a coefficient which is a function of both wind and wave fields. Hasselmann evaluated η_b indirectly by computing the energy balance of the high frequency portion of a wave spectrum, then applied it to the entire spectrum. Because the parameterized nonlinear energy transfer equation does not give accurate results for the high frequency waves, Hasselmann's method for evaluating η_b is not expected to give accurate results in the proposed model. Therefore, it is not used.

IV.F. Wind Generation

From the discussion in Chapter II, A, Dobson and Elliott's (1977) results from the joint experiment in the Bight of Abaco,

$$\beta = 0.25\ (U_5 \cos \theta_w / c - 1) \quad ,$$

sufficiently approximates the average of results derived from several field measurements and theoretical calculations. For this reason, it will be used in the model developed here.

CHAPTER V

NUMERICAL SOLUTION OF THE ENERGY EQUATION IN FINITE-DEPTH WATER

V.A. Energy Balance Equation

The evolution of a slowly varying wave field is governed by the equation of the conservation of action density,

$$\frac{DA_c}{Dt} = \frac{\partial A_c}{\partial t} + \dot{x}_i \frac{\partial A_c}{\partial x_i} + \dot{k}_i \frac{\partial A_c}{\partial k_i} = \frac{S}{\omega} \quad , \quad i = 1, 2 \quad , \tag{5-1}$$

where $A_c = A_c(t,\vec{x},\vec{k})$, is the action density defined by $F(t,\vec{x},\vec{k})/\omega$, F is the two-dimensional wave number spectrum, $\omega = (gk \tanh kh)^{1/2}$, t is time, x_1 and x_2 are the horizontal coordinates, k_1 and k_2 are the wave number components in the x_1 and x_2 directions respectively, $k = |\vec{k}| = (k_1^2 + k_2^2)^{1/2}$, the dot denotes the time derivative, and S is the source function representing the net energy transfer to or from the wave spectrum at wave number k.

Equation (5-1) describes the change of wave action density along the path of the wave group in the $\vec{x}$-$\vec{k}$ plane and is a general equation that allows for the inclusion of space- and time-dependent current, and water depth. The derivation of Equation (5-1) can be found in Willebrand (1975).

If ω is constant along the wave path, Equation (5-1) becomes

$$\frac{DF}{Dt} = \frac{\partial F}{\partial t} + \dot{x}_i \frac{\partial F}{\partial x_i} + \dot{k}_i \frac{\partial F}{\partial k_i} = S \quad , \quad i = 1, 2 \quad . \tag{5-2}$$

In Equations (5-1) and (5-2)

$$\dot{x}_i = \frac{\partial \omega'}{\partial k_i} = V_i \quad , \tag{5-3}$$

is the group velocity, where

$$\omega' = (gk \tanh kh)^{1/2} + \vec{U}_c \cdot \vec{k} \tag{5-4}$$

$$= \omega + \vec{U}_c \cdot \vec{k} \quad ,$$

and $\vec{U}_c$ is the current velocity; and

$$\dot{k}_i = - \frac{\partial \omega}{\partial x_i} \quad ,$$

represents the conservation of waves (Phillips, 1969). If U_c is negligibly small ($|\vec{U}_c| << c$) and the wave field is stationary, Equation (5-2) becomes

$$V_i \frac{\partial F}{\partial x_i} = S \quad . \tag{5-5}$$

Furthermore, if the wave field and the bottom topography are homogeneous in the y direction, then Equation (5-5) becomes

$$V \cos \theta \frac{dF}{dx} = S \quad , \tag{5-6}$$

where θ and x are defined in Figure 23, and $V = |\vec{V}|$ is the absolute value of group velocity.

Let $E(t, \vec{x}, f, \theta)$ be the two-dimensional wave frequency spectrum, where f is frequency in hertz. From the definition of E and F, $Edfd\theta = Fdkd\theta$, the relationship between E and F can be found as

$$F = \frac{V}{2\pi k} E \quad . \tag{5-7}$$

Now Equation (5-6) becomes

$$\frac{V \cos \theta}{2\pi} \frac{d}{dx} \left(\frac{VE}{k} \right) = S \quad , \tag{5-8}$$

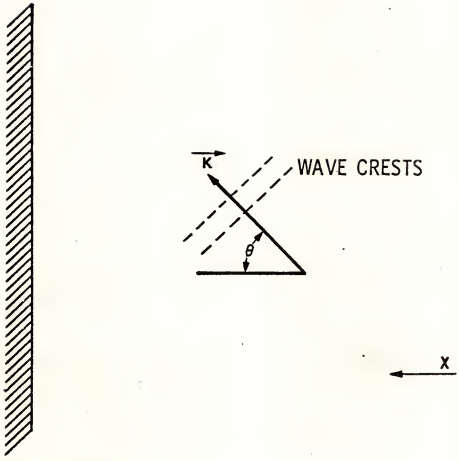

Figure 23. Definition Sketch.

or

$$\frac{dE}{dx} = E\left(\frac{1}{k}\frac{dk}{dx} - \frac{1}{V}\frac{dV}{dx}\right) + \frac{2\pi k}{V^2 \cos\theta} S \quad . \tag{5-9}$$

Equation (5-9) is the equation used in the model developed here.

V.B. Refraction and Shoaling

As waves propagate towards shore, they begin to feel the bottom at a water depth equal to one half of the wave length. The bottom effect induces changes in wave length, group velocity, wave direction, and orbital wave properties. The changes in wave direction and group velocity then modify the wave energy. These effects are called refraction and shoaling respectively. Refraction and shoaling are energy conserving processes, i.e., no wave energy is generated or dissipated through these processes. The wave energy is simply redistributed.

In the energy balance equation given in Equation (5-9) the term $-(E/V)dV/dx$ represents shoaling and the term $(E/k)dk/dx$ represents refraction. These can be explained by the following demonstration. If S is zero, Equation (5-8) becomes

$$\frac{EV}{k} = \text{constant} = \frac{E'V'}{k'} \quad . \tag{5-10}$$

Now, the wave spectrum is affected by only refraction and shoaling. Snell's Law for wave refraction describes that along the wave ray,

$$k \sin\theta = k' \sin\theta' = \text{constant} \quad ,$$

or

$$k \cos\theta\Delta\theta = k' \cos\theta' \Delta\theta' \quad . \tag{5-11}$$

By using Equation (5-11), Equation (5-10) becomes

$$EV \cos\theta\Delta\theta = E'V' \cos\theta' \Delta\theta' \quad . \tag{5-12}$$

Multiplying Equation (5-12) by Δf and letting $E\Delta\theta\Delta f = E_m$, it becomes

$$E_m V \cos\theta = E_m{}' V' \cos\theta' \quad . \tag{5-13}$$

This is the conventional wave energy conservation equation for parallel bottom contours, in which V represents the shoaling effect and cos θ represents the refraction effect. Referring back to Equation (5-10), it can be seen that cos θ in Equation (5-13) corresponds to k in Equation (5-10). Therefore, the terms with dV/dx and dk/dx in Equation (5-9) describe the effects of shoaling and refraction respectively.

In Equation (5-9), the variations of k and V with respect to x can be written as

$$\frac{dk}{dx} = -\frac{dh}{dx}\frac{1}{V}\frac{\partial\omega}{\partial h} \quad , \tag{4-39}$$

$$\frac{dV}{dx} = \frac{\partial V}{\partial k}\frac{dk}{dx} + \frac{\partial V}{\partial h}\frac{dh}{dx} \quad , \tag{5-15}$$

where dh/dx is the slope of the bottom.

By using the dispersion equation, $\omega^2 = gk \tanh kh$, some of the terms in Equations (5-14) and (5-15) become

$$\frac{\partial\omega}{\partial h} = \frac{gk^2}{2\omega} - \frac{\omega^3}{2g} \quad , \tag{5-16}$$

$$\frac{\partial V}{\partial k} = \frac{\partial^2\omega}{\partial k^2} = \frac{\partial^2\omega}{\partial k\partial h}\frac{h}{k} - \frac{1}{2k}\frac{\partial\omega}{\partial k} \quad , \tag{5-17}$$

$$\frac{\partial V}{\partial h} = \frac{\partial^2\omega}{\partial h\partial k} = \frac{\partial^2\omega}{\partial h^2}\frac{h}{k} + \frac{3}{2k}\frac{\partial\omega}{\partial h} \quad , \tag{5-18}$$

where

$$V = \frac{\partial\omega}{\partial k} = \frac{1}{2}\frac{\omega}{k} + \frac{h}{k}\frac{\partial\omega}{\partial h} \quad , \tag{5-19}$$

and

$$\frac{\partial^2\omega}{\partial h^2} = \frac{\partial\omega}{\partial h}\left(-\frac{gk^2}{2\omega^2} - \frac{3}{2}\frac{\omega^2}{g}\right) . \tag{5-20}$$

Thus refraction and shoaling can be computed in Equation (5-9).

V.C. Source Functions

The source function, S, can be written as

$$S = S_n + S_m + S_f + S_p + S_g \quad , \tag{5-21}$$

where the subscripts n, m, f, p, and g refer to nonlinear transfer, mud dissipation, friction, percolation, and generation respectively.

From Equation (4-1)

$$S_n = (\Gamma - \xi E)\frac{V}{2\pi k} \quad , \tag{5-22}$$

where Γ and ξ are defined in Equations (4-2) and (4-3).

For mud dissipation, the real part of the wave number is assumed to be equal to the wave number found in a firm bottom in order to simplify the computation. The source function in terms of k_i is

$$S_m = -\frac{1}{\pi}\frac{k_i}{k}\frac{E}{\cos\theta} \quad , \tag{5-23}$$

where k_i is given by (4-17).

From Equations (4-23) and (4-24),

$$S_f = \frac{gC_f}{\omega^2\cosh^2 kh}\left[k^2\left\langle|\vec{W}|\right\rangle + 2k_1k_2\left\langle\frac{W_1W_2}{|\vec{W}|}\right\rangle\right]\frac{EV}{2\pi k} \quad . \tag{5-24}$$

From Equation (4-32),

$$S_p = -Ek\sqrt{k_xk_z}\tanh\left(\frac{k_x}{k_z}kd\right)\cdot V/(2\pi k\cosh^2 kh) \quad . \tag{5-25}$$

For wind generation,

$$S_g = \beta \frac{\rho_a}{\rho_w} \omega E \frac{V}{2\pi k} \quad , \tag{5-26}$$

where

$$\beta = 0.25 \ (U_5 \cos \theta_w / c - 1) \quad . \tag{2-8}$$

The effect of wave breaking is taken into account by setting the upper limit of the spectrum as

$$E(f) = \frac{\alpha_e g^2}{(2\pi)^4 f^5} \exp \left[-0.74 \left(\frac{f_w}{f} \right)^4 \right] \quad , \tag{4-34}$$

where $\alpha_e = 0.076 \left(F_x g / U_{10}^2 \right)^{-0.22}$.

V.D. Numerical Computations

The equation to be solved in the model can be written in the form of

$$\frac{dE(f, \theta)}{dx} = M \cdot E(f, \theta) + N \quad , \tag{5-27}$$

where M and N are functions of x, f, θ and the entire spectrum. It is assumed that M and N are slowly varying functions of x, i.e.,

$$M(x) \cong M(x = x_o) = M_o \quad ,$$

$$N(x) \cong N(x = x_o) = N_o \quad ,$$

within range $x_o \leq x \leq x_o + \Delta x$. Then the solution of Equation (5-27) in the interval $[x_o, x_o + \Delta x]$ is approximately

$$E(x) = \frac{N_o}{M_o} \left(e^{M_o (x - x_o)} - 1 \right) + E(x_o) \, e^{M_o (x - x_o)} \quad . \tag{5-28}$$

For $x = x_o + \Delta x$,

$$E(x_o + \Delta x) = \frac{N_o}{M_o}\left(e^{M_o \Delta x} - 1\right) + E(x_o)\, e^{M_o \Delta x} \quad . \tag{5-29}$$

Equation (5-29) can be rewritten as

$$\Delta E = \left(\frac{N_o}{M_o} + E(x_o)\right)\left(e^{M_o \Delta x} - 1\right) \quad , \tag{5-30}$$

where $\Delta E = E(x_o + \Delta x) - E(x_o)$. If $M_o = 0$, then

$$\Delta E = N_o \Delta x \quad . \tag{5-31}$$

Applying Equations (5-19) and (5-20), the computation procedures used in the model are:

$$\Delta E_1 = \Delta E\,(E(x_o),\ M(x_o),\ N(x_o)) \quad ,$$

$$\hat{E}(x_o + \Delta x) = E(x_o) + \Delta E_1 \quad , \tag{5-32}$$

$$\Delta E_2 = \Delta E\,(\hat{E}(x_o + \Delta x),\ M(x_o + \Delta x),\ N(x_o + \Delta x)) \quad ,$$

$$E(x_o + \Delta x) = E(x_o) + \frac{1}{2}(\Delta E_1 + \Delta E_2) \quad ,$$

which is a second order Runge-Kutta type method.

This numerical scheme is tested by running the model without the source function, i.e., with only energy conserving processes. The conservation of wave energy under refraction and shoaling is then examined. For the test case in which the water depth decreases from 40 m to 10 m with a constant slope of 0.00065, the numerical errors are less than 2% with $\Delta x = 2000$ m for wave periods in the range 4 to 16 seconds. The numerical accuracy is different for different depth profiles. In each of the geographic areas where the model is applied, this test is used to determine an appropriate Δx to keep the numerical errors reasonably small.

CHAPTER VI

RESULTS AND VERIFICATIONS

The wave data taken from offshore of Marineland and Panama City, Florida; Melkbosstrand, South Africa; offshore of the middle Atlantic states; and East Bay, Louisiana, are available for intercomparison and for verifying the model. The data from Marineland, Panama City, and Melkbosstrand suggest that bottom friction is the major wave transform mechanism. The friction coefficients which give the best fit between predictions and measurements are compared with those estimated independently from the friction factor diagram. The wave data set obtained in the Atlantic corresponds to an ideal generation case. The mechanisms of wind generation, nonlinear energy transfer, and wave breaking are conveniently tested by using this set of data. Finally, the East Bay wave data set is used to test the mud movement mechanism. The predictions are compared with the measurements.

VI.A. Marineland Experiment

A major experiment was conducted on the continental shelf offshore of Marineland, Florida, during the last week of November and the first two weeks of December, 1975 (Shemdin, Blue, and Dunne, 1975). It was a multi-purpose experiment conducted by fifteen organizations including the Coastal and Oceanographic Engineering Laboratory, University of Florida. The test area is shown in Figure 24. During this experiment period, several days of good data were obtained but only the data on

Figure 24. Marineland test area and bottom profile.

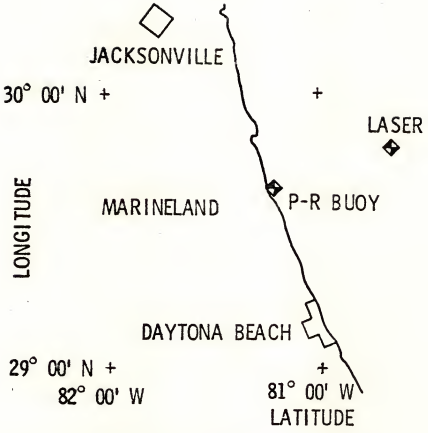
JACKSONVILLE
30° 00' N +
+
LASER
LONGITUDE
MARINELAND
P-R BUOY
DAYTONA BEACH
29° 00' N +
+
82° 00' W
81° 00' W
LATITUDE

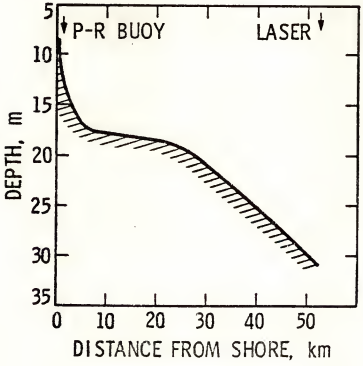
P-R BUOY
LASER
DEPTH, m
5
10
15
20
25
30
35
0
10
20
30
40
50
DISTANCE FROM SHORE, km

December 14 are suitable for this study. On that day there were Geodolite laser measurements obtained at a depth 31 m and pitch-and-roll buoy and pressure gage measurements obtained at a depth 8.5 m. The wave spectra measured by the pitch-and-roll buoy and the pressure gage were compared. The agreement was found to be satisfactory (Figure 25).

The bottom sediment in this area is mostly very fine to fine, poorly-sorted silty quartz sand (Meisburger and Field, 1975). The percolation loss is negligibly small compared to friction loss.

The best fit between computation and measurement gives a friction coefficient of 0.008 (Figure 26). In using the significant wave height and period, Dingler's (1975) ripple study results and the friction factor diagram of Kamphuis (1975) show the estimated friction coefficients to be 0.002 at 8.5 m water depth and 0.05 at 31 m water depth (Table 1). Since the friction coefficient changes rapidly in this case the spectrum was recomputed using a variable friction coefficient estimated from Dingler's study and the friction factor diagram. A very good agreement is obtained between the computed and measured spectra at 8.5 m water depth as shown in Figure 26.

VI.B. Panama City Data

The Panama City data were obtained with two pressure sensor arrays which were operated by the Naval Coastal Systems Laboratory to measure the directional wave spectra (Breeding, 1972). The array configuration used consists of one sensor at each corner of a pentagon 35.8 m on a side, and a sixth sensor at the center of the pentagon at a distance of 30.5 m from the other sensors. The arrays were placed on the sea floor at the sites of two offshore stages. Stage I is located 17.7 km from

Figure 25. Comparison between measured wave spectra at 8.5 m depth water, Marineland, Florida. NOAA - pitch-and-roll buoy measurement, UF - pressure measurement.

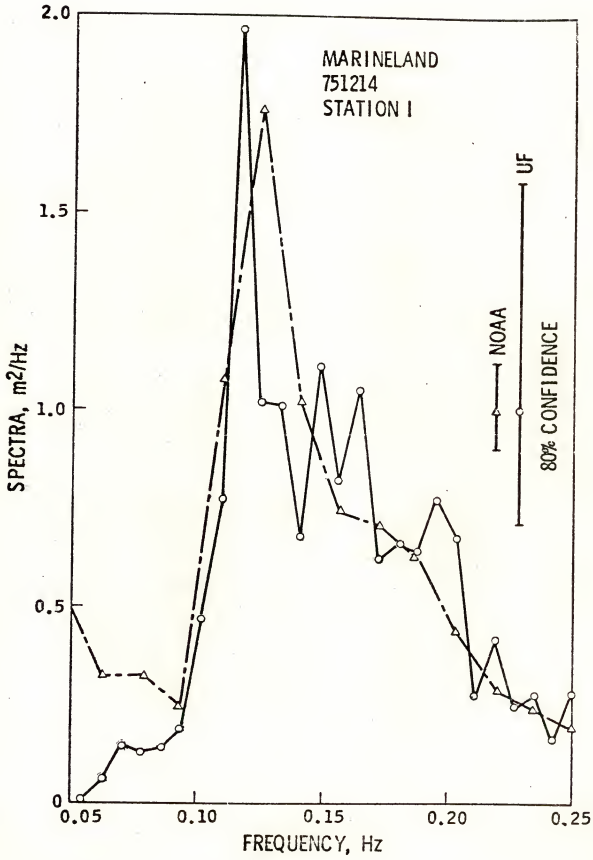
MARINELAND
751214
STATION I
NOAA
UF
80% CONFIDENCE
SPECTRA, m²/Hz
FREQUENCY, Hz
2.0
1.5
1.0
0.5
0
0.05
0.10
0.15
0.20
0.25

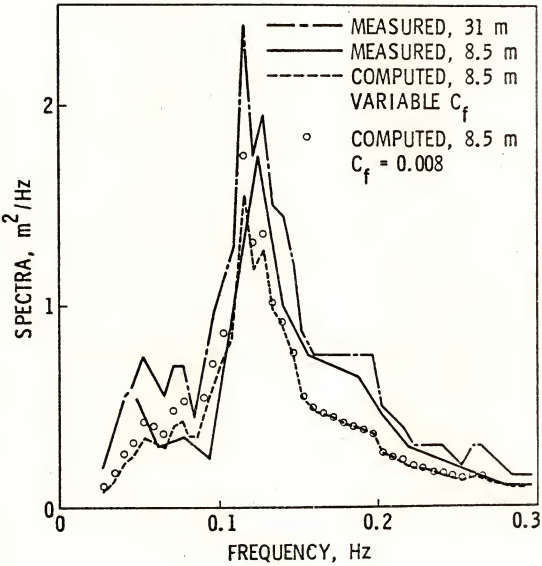

Figure 26. Comparison between measured and computed Marineland wave spectra.

shore where the water depth is 31.7 m. Stage II is located 3.2 km from shore where the water depth is 19.2 m. The locations are shown in Figure 27. The configuration and water depths were chosen to optimize the detection of waves with periods in the range 6 to 10 seconds. For waves with periods less than 6 seconds the signals produced by the waves are below the noise level at Stage I because of the pressure attenuation with water depth. At Stage II, the signals for waves with less than 5 second period are below the noise level. Wave height spectra are obtained by dividing the pressure spectra by the attenuation factor, cosh kh. At high frequency, the noise in the pressure signal is magnified by the attenuation factor. The corresponding wave height spectra have large high frequency tails as shown in Figure 28. To offset this problem, the spectra were fitted with f^{-5} high frequency tails.

The bottom sediment in this area is mostly sand with a median diameter of about 0.4 mm and with a thickness of 4-8 m (Tolbert and Austin, 1959, and McLeroy, 1972). The percolation dissipation was computed based on a coefficient of permeability equal to 0.0015 m/sec and a sand layer of 7 m thick. It was found to be negligible compared to friction dissipation.

The results of computation for seven spectra measured on September 9, 1965 are shown in Figures 29 to 35. The time difference selected between Stages I and II represents the travel time of the dominant waves from Stage I to Stage II. The friction coefficients which give the best fit between the computed spectra and the measured spectra at Stage II fall in the range 0.035 to 0.05. These are of the same order of magnitude as the estimated 0.03 from Dingler's ripple study results and the friction factor diagram.

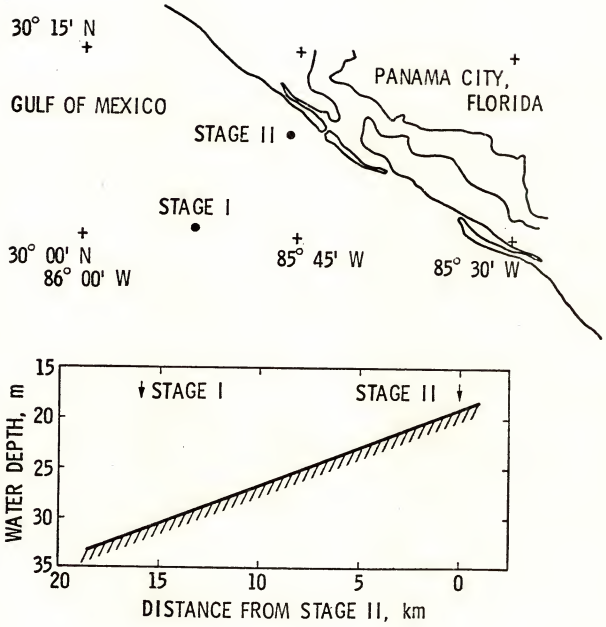

Figure 27. Panama City test area and bottom profile.

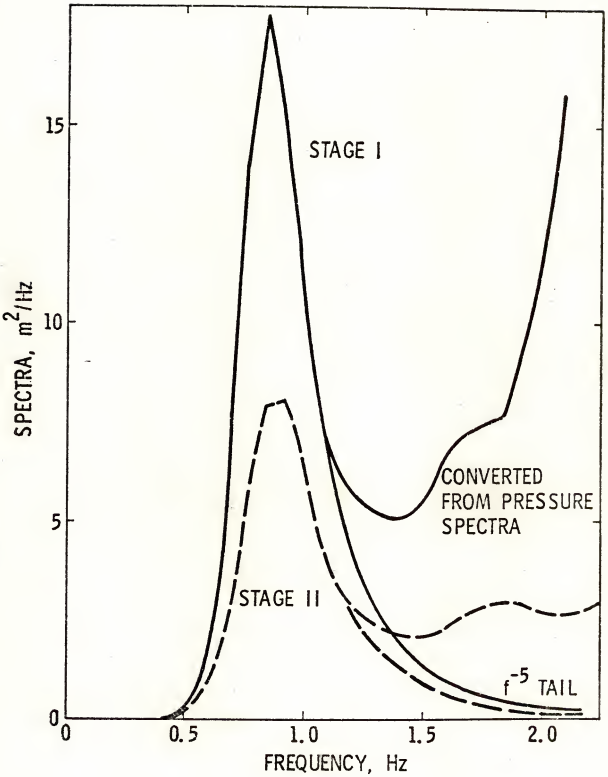

Figure 28. Examples of the f^{-5} tail spectra, measured during 1144-1215 local time, September 9, 1965.

Figure 29. Comparison between measured and computed Panama City wave spectra, September 9, 1965.

a) ——— Measured, Stage I (local time 0903-0935) and computed, Stage II.

b) ---- Measured, Stage II (local time 0936-1007).

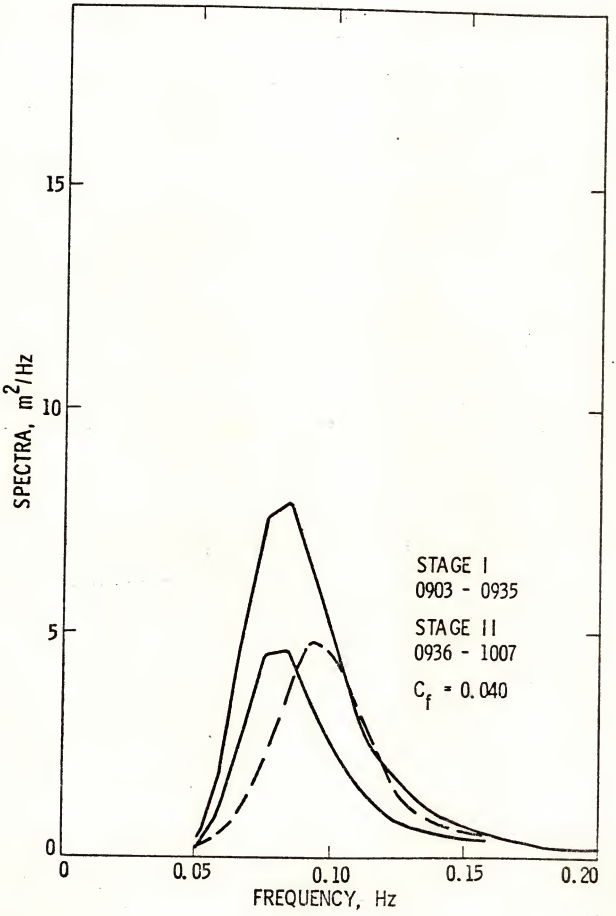
15
10
5
0
SPECTRA, m²/Hz
0
0.05
0.10
0.15
0.20
FREQUENCY, Hz
STAGE I
0903 - 0935
STAGE II
0936 - 1007
C_f = 0.040

Figure 30. Comparison between measured and computed Panama City wave spectra, September 9, 1965.

a) ——— Measured, Stage I (local time 0936-1007) and computed, Stage II.

b) ---- Measured, Stage II (local time 1008-1039).

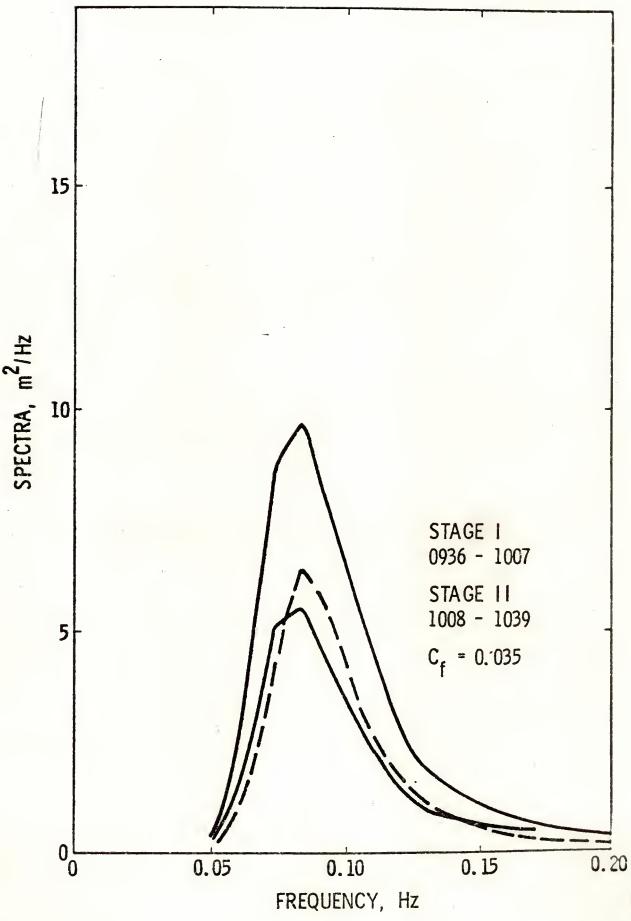
SPECTRA, m²/Hz
15
10
5
0
0
0.05
0.10
0.15
0.20
FREQUENCY, Hz
STAGE I
0936 - 1007
STAGE II
1008 - 1039
C_f = 0.035

Figure 31. Comparison between measured and computed Panama City wave spectra, September 9, 1965.

a) ——— Measured, Stage I (local time 1008-1039) and computed, Stage II.

b) ---- Measured, Stage II (local time 1040-1111).

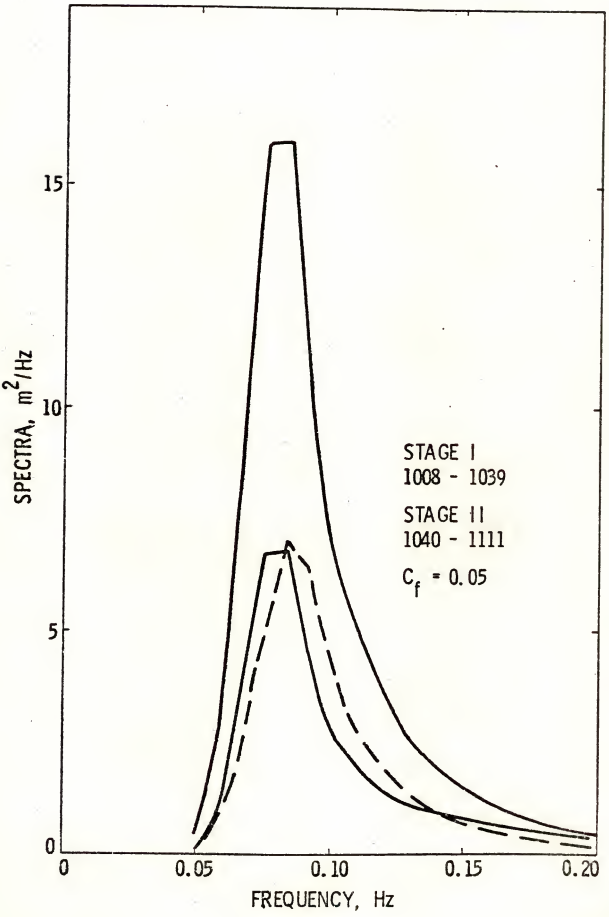
SPECTRA, m²/Hz
15
10
5
0
0
0.05
0.10
0.15
0.20
FREQUENCY, Hz
STAGE I
1008 - 1039
STAGE II
1040 - 1111
C_f = 0.05

Figure 32. Comparison between measured and computed Panama City wave spectra, September 9, 1965.

a) ——— Measured, Stage I (local time 1112-1143) and computed, Stage II.

b) ---- Measured, Stage II (local time 1144-1215).

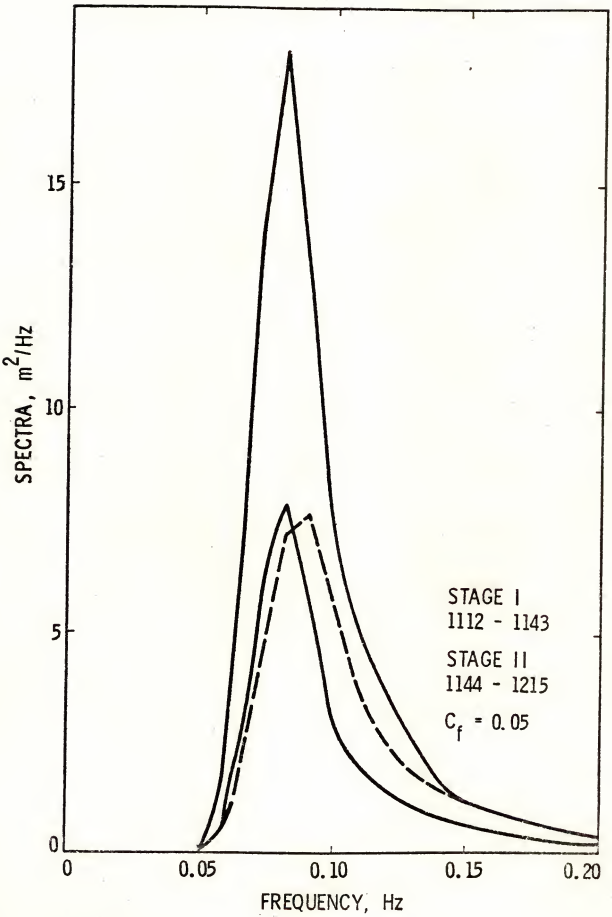
SPECTRA, m²/Hz
15
10
5
0
0
0.05
0.10
0.15
0.20
FREQUENCY, Hz
STAGE I
1112 - 1143
STAGE II
1144 - 1215
C_f = 0.05

Figure 33. Comparison between measured and computed Panama City wave spectra, September 9, 1965.

a) ——— Measured, Stage I (local time 1144-1215) and computed, Stage II.

b) ---- Measured, Stage II (local time 1216-1247).

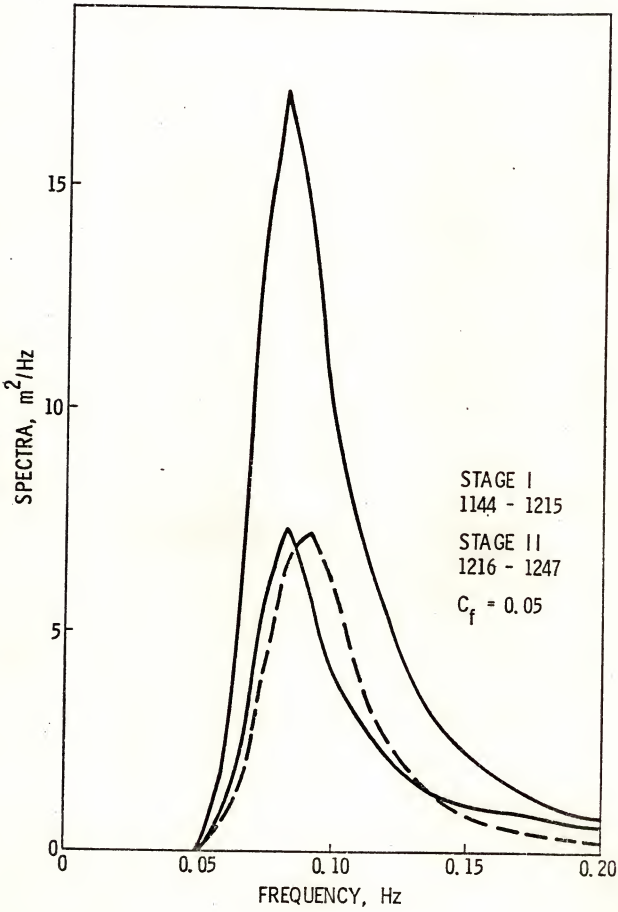
SPECTRA, m²/Hz
15
10
5
0
0
0.05
0.10
0.15
0.20
FREQUENCY, Hz
STAGE I
1144 - 1215
STAGE II
1216 - 1247
C_f = 0.05

Figure 34. Comparison between measured and computed Panama City wave spectra, September 9, 1965.

a) —— Measured, Stage I (local time 1216-1247) and computed, Stage II.

b) ---- Measured, Stage II (local time 1248-1319).

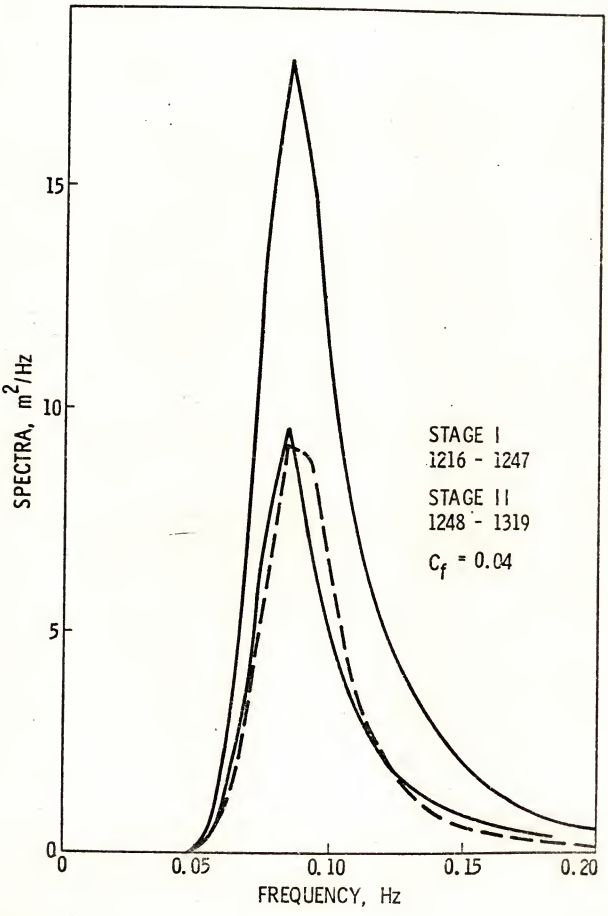
SPECTRA, m²/Hz
15
10
5
0
0
0.05
0.10
0.15
0.20
FREQUENCY, Hz
STAGE I
1216 - 1247
STAGE II
1248 - 1319
C_f = 0.04

Figure 35. Comparison between measured and computed Panama City wave spectra, September 9, 1965.

a) ——— Measured, Stage I (local time 1248-1319) and computed, Stage II.

b) ---- Measured, Stage II (local time 1320-1352).

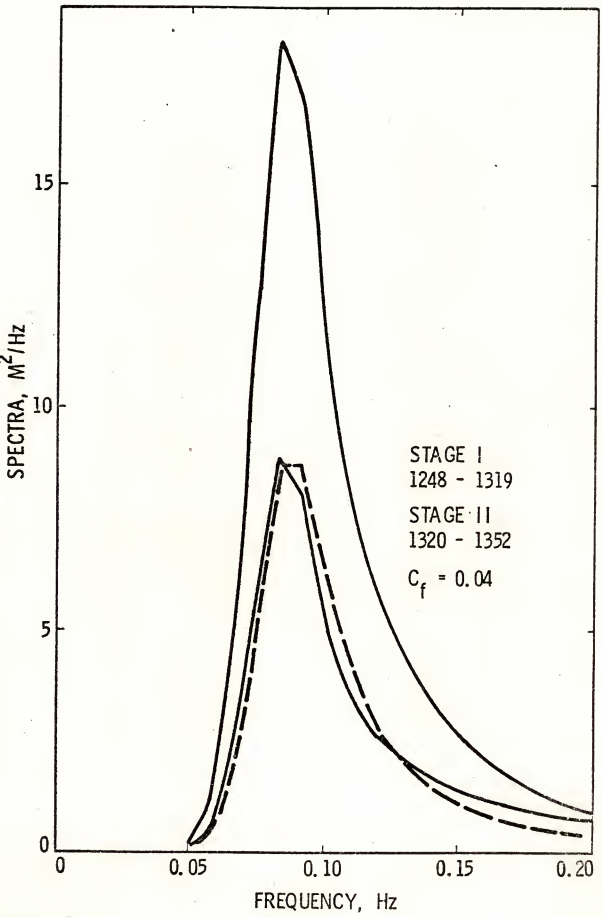
SPECTRA, M^2/Hz
15
10
5
0
0
0.05
0.10
0.15
0.20
FREQUENCY, Hz
STAGE I
1248 - 1319
STAGE II
1320 - 1352
C_f = 0.04

VI.C. South Africa Data

From January 1969 until February 1970 wave records were obtained by Van Ieperen (1975) each month at Melkbosstrand near Cape Town, South Africa (see Figure 36). The data were taken by a ship-borne wave recorder at stations with depths 45, 32, 19.8, and 10.6 m. The corresponding distances between the stations were 1.6, 1.6, and 1.3 km respectively. The directions of waves were measured with the ship's Gyro compass which had an error of ±10°.

Van Ieperen (1975) obtained friction coefficients from the significant wave heights and from the integrated spectra separately. He considered only shoaling and friction in his computations. One case of his wave data sets (TBO 37) is examined here for comparison. For this data set he found $C_f = 0.09$ from significant wave heights and $C_f = 0.073$ from integrated spectra. The proposed model yields $C_f = 0.12$ for the fits shown in Figure 37. The differences in C_f are mainly due to the differences in the methods of analysis.

Not enough data on the sea bottom is available for this area. It is assumed that the bottom is composed of firm sand as stated in Van Ieperen's (1975) paper. If the sand is coarse, say with a median diameter of 1.5 mm, the estimated value of C_f from Dingler (1975) and Kamphuis (1975) is 0.10. Because this friction coefficient is large the percolation effect is minor compared to the friction dissipation even in coarse sand. A summary of the wave and bottom parameters and the corresponding friction coefficients for the above three cases is shown in Table 1.

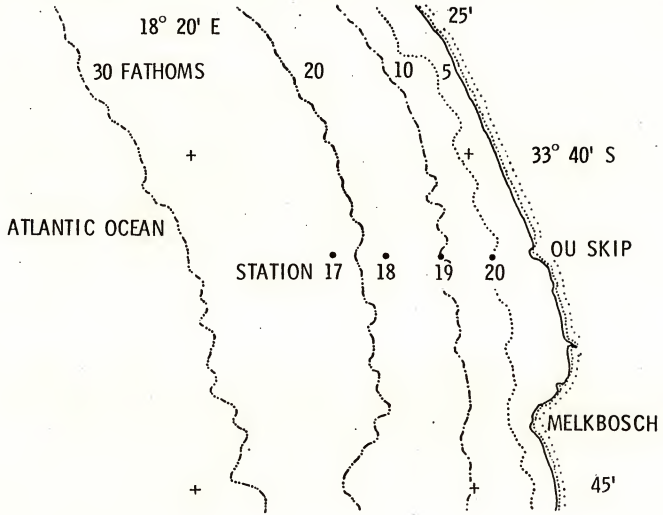

Figure 36. South Africa test area [After Van Ieperen (1975)].

Figure 37. Comparison between measured and computed South Africa wave spectra.

a) ——— Measured.

b) ---- Computed.

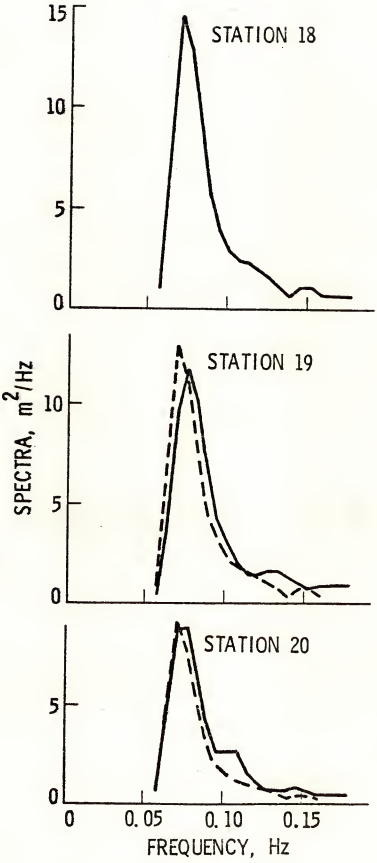
STATION 18
STATION 19
STATION 20
SPECTRA, m²/Hz
FREQUENCY, Hz
15
10
5
0
0.05
0.10
0.15

Table 1. Estimation of Friction Coefficients from Wave and Sand Parameters

	Marineland		Panama City	South Africa (TBO 37)
h	30	8.5	19.2 - 31.7	10.6 - 32
T_m	8	8	12	13.7
$H_{1/3}$	1.7	1.5	1.9 - 3.7	2.3 - 2.8
d_o	0.49	1.68	1.9 - 2.9	2.6 - 4.5
D_s	0.1×10^{-3}		0.4×10^{-3}	1.5×10^{-3}
λ_s	0.070	0.032	0.24	0.9
θ_s	24	290	33 - 82	15 - 45
ζ	0.012	0	0.024	0.15
k_s	0.048	0.0001	0.096	0.60
C_f	0.05	0.002	0.03	0.10

h = water depth (m)

T_m = peak period (sec)

$H_{1/3}$ = significant wave height (m)

d_o = horizontal excursion (m)

D_s = median sand diameter (m)

λ_s = ripple wave length (m)

θ_s = nondimensional relative stress

ζ = ripple wave height (m)

k_s = roughness height (m)
(4ζ as was suggested by Jonsson, 1966)

C_f = friction coefficient

VI.D. Atlantic Wave Data

This set of data was measured by Barnett (1966) using an airborne radar wave profiler. Waves from the coast out to a distance of 190 nautical miles were measured after a steady offshore wind of 30-35 knots had been blowing for at least 12 hours from a direction of 335° from true North. This is an ideal case for verifying the wave growth mechanisms of wind generation, nonlinear energy transfer, and wave breaking. The spectrum at 175 nautical miles offshore was computed from the spectrum at 50 nautical miles offshore. For a wind speed of 17.0 m/sec (33 knot) the computed spectrum matches the measured spectrum very well (Figure 38).

The wind input used in this model is based on the recent theoretical and experimental studies and it is much smaller than those used in the previous models. The computation shown in Figure 38 indicates that the wave growth measured in the field can be explained successfully by the latest findings on wind input, nonlinear transfer, and wave breaking.

VI.E. East Bay Wave Data

Wave measurements in East Bay, Louisiana, obtained by Tubman and Suhayda (1976), are used to verify the mud dissipation theory. Waves were measured at 19.2 m and 5.3 m depths where the bottom consisted of soft mud uniformly.

Test cores of this kind of bottom material were taken in the Gulf of Mexico by Carpenter, Thompson, and Bryant (1973). An analysis of these data has shown that when the shear strain and the rate of shear strain are on the order of the wave motion, the viscosity, ν, of the mud

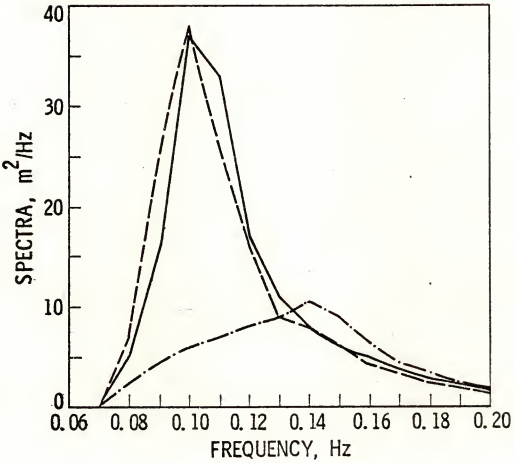

Figure 38. Comparison between measured and computed Atlantic spectra.

a) - · - Measured at 50 nautical mile fetch.
b) ----- Measured at 175 nautical mile fetch.
c) ——— Computed at 175 nautical mile fetch.

is of the order of 0.5 m^2/sec, and the ratio of the shear modulus to density of mud, J, is of the order of 10 m^2/sec^2.

The computed wave energy dissipation based on a mud depth of 2 m, with $\nu = 0.6$ m^2/sec, and $J = 10$ m^2/sec^2 is shown in Figure 39. A computation with the bottom friction by Tubman and Suhayda (1976) is also shown for comparison. It can be seen from the figure that the excessive wave energy dissipation can be predicted by using the visco-elastic mud model. This excessive energy dissipation can not be explained by bottom friction with a moderate friction coefficient. A high friction coefficient is unlikely in this area because of the presence of fine sediment.

Figure 39. Soft bottom effects on water wave height.

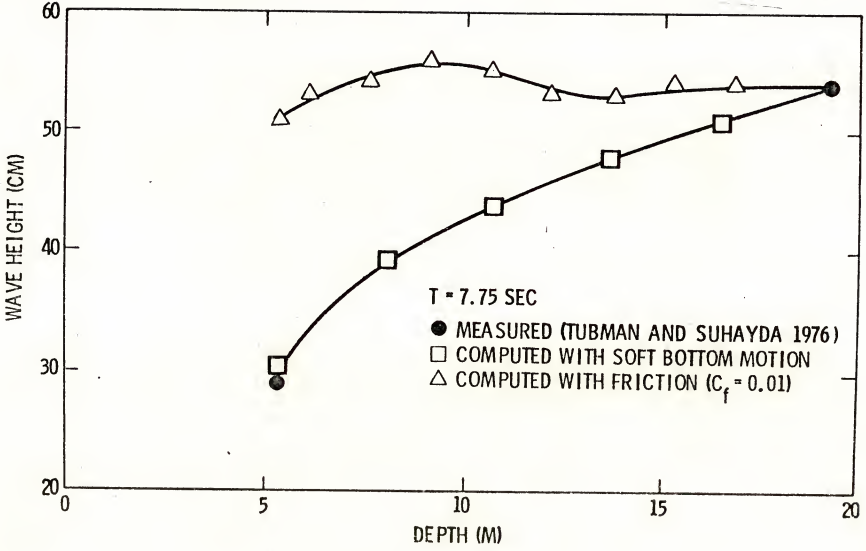
60
50
40
30
20
0
5
10
15
20
WAVE HEIGHT (CM)
DEPTH (M)
T = 7.75 SEC
MEASURED (TUBMAN AND SUHAYDA 1976)
COMPUTED WITH SOFT BOTTOM MOTION
COMPUTED WITH FRICTION (C_f = 0.01)

CHAPTER VII

CONCLUSION

A model has been developed for predicting the two-dimensional wave spectrum in finite depth water. This model uses the energy equation and six wave transformation mechanisms to calculate the evolution of the wave spectrum in finite-depth water. The mathematical formulation for each mechanism was developed based on the most recent theories and experimental results available. Comparisons between computations and measurements show good agreement. The important conclusions of this dissertation are summarized below:

(i) The nonlinear energy transfer is an important wave transformation mechanism in shallow water.

(ii) For waves propagating over a flexible bottom the viscoelastic model can explain the excessive energy dissipation which can not be accounted for by bottom friction.

(iii) The friction coefficient is not a constant. Its value depends on the wave and bottom sediment conditions.

(iv) Percolation can be an important dissipation mechanism when the bottom sand is coarse.

(v) The wind wave growth depends on the mechanisms of wind generation, nonlinear transfer, and wave breaking. The proposed model can explain the growth of waves measured in the field.

CHAPTER VIII

RECOMMENDATIONS

The progress made to date in the finite-depth water wave prediction reveals a number of avenues for future research. These are summarized below:

(i) In this model the nonlinear energy transfer is computed by using the deep water wave parameterized equation and adjusted for finite depth water waves. The direct theoretical computation of nonlinear source function for finite depth water wave spectra is desirable for checking the computation method used in this model or for developing a parameterized equation which can be used directly to compute the nonlinear transfer for a finite depth water wave spectrum.

(ii) The parameterized equation for nonlinear energy transfer is obtained on the basis of the theoretically computed nonlinear source functions for the spectra with peaks at 0.3 Hz frequency. Although the effect of the frequency scale is considered in the parameterized equation, it needs to be verified by the theoretically computed nonlinear source functions for spectra with different peak frequencies.

(iii) The present knowledge on the mechanical properties of the flexible sea bottoms is not adequate. Future investigations on the stress-strain relationship of soft bottom material are required to define the mechanical properties more precisely. Besides, more wave

measurements of different dominant frequencies and different energy levels with simultaneous measurements of bottom movement are required for a better understanding of the interaction between waves and the bottom.

(iv) To date, all the bottom friction and ripple formation measurements are obtained only for monochromatic waves or very narrow wave spectra. Measurements are needed for wind wave spectra or non-dispersed swell spectra for determining friction coefficients in such cases.

(v) How the non-wave-induced current affects the ripple formation and how the current generated ripple affect the friction coefficient are not known yet. Studies on these aspects are needed for a better understanding of the relationships between ripples and friction coefficients.

(vi) The assumption of parallel bottom contours is reasonably good for many coastal areas. However, there are areas where the bottom contours are not regular. A two-dimensional model is required for the wave prediction in such areas. The mathematical formulations in this model can be extended to a two-dimensional model. However, the computation techniques will be much more complicated and the computation time will increase significantly.

APPENDIX

THE DERIVATION OF FRICTION DISSIPATION EQUATION

The energy dissipation due to bottom friction of a wave component with wave number $\vec{k}$ is given by the work done by the total bottom stress, $\vec{\tau}$, against the bottom orbital velocity, $\vec{U}_{\vec{k}}$, of the wave component with wave number $\vec{k}$, i.e.,

$$\rho g \frac{\partial F(\vec{k})}{\partial t} \Delta\vec{k} = < \vec{\tau} \cdot \vec{U}_{\vec{k}} > = < \tau_i U_{i\vec{k}} > \quad , \tag{1}$$

where < > denotes the ensemble average, ρ is the water density, g is the gravitational acceleration, t is time, and F is the wave spectrum. In order to simplify the notation, $\vec{U}$ will be used in place of $\vec{U}_{\vec{k}}$.

The quadratic friction law states

$$\vec{\tau} = -\rho \, C_f \, \vec{u} \, | \, \vec{u} \, | \quad , \tag{2}$$

where C_f is the friction coefficient and $\vec{u}$ is the total bottom velocity including current and orbital velocities of all the wave components. The term $\vec{u}$ can be written as

$$\vec{u} = \vec{u}' + \vec{U} \quad , \tag{3}$$

where $\vec{u}'$ is the total bottom velocity excluding $\vec{U}$. If $\Delta\vec{k}$ is small enough, then $|\vec{U}| << |\vec{u}|$ and $\vec{u}' \cong \vec{u}$. From Equation (3)

$$|\vec{u}| = |\vec{u}' + \vec{U}| = [u'^2 + U^2 + 2u' U \cos \alpha]^{1/2} \quad , \tag{4}$$

where u' and U are the absolute values of $\vec{u}'$ and $\vec{U}$ respectively and α is the angle between $\vec{u}'$ and $\vec{U}$. Since U << u, Equation (4) becomes

$$|\vec{u}| \cong [u'^2 + 2u' U \cos\alpha]^{1/2}$$

$$= u' + \frac{1}{2}\frac{2u' U \cos\alpha}{u'} + \text{Higher order terms}$$

$$\cong u' + \frac{\vec{u}' \cdot \vec{U}}{u'^2}$$

$$= u' \left(1 + \frac{\vec{u}' \cdot \vec{U}}{u'^2}\right) . \qquad (5)$$

Then Equation (2) becomes

$$\vec{\tau} = -\rho C_f u' \left(1 + \frac{\vec{u}' \cdot \vec{U}}{u'^2}\right) (\vec{u}' + \vec{U}) \quad ,$$

or

$$\tau_i = -\rho C_f u' \left(1 + \frac{\vec{u}' \cdot \vec{U}}{u'^2}\right) (u_i' + U_i) \quad . \qquad (6)$$

Substituting Equation (6) into Equation (1), it follows

$$\rho g \frac{\partial F(\vec{k})}{\partial t} \Delta\vec{k} = -\rho C_f < u' (u_i' + U_i) \left(1 + \frac{u_j' U_j}{u'^2}\right) U_i >$$

$$= -\rho C_f < u' \left(u_i' U_i + U_i U_i + \frac{u_i' u_j' U_i U_j}{u'^2} + \text{H.O.T.}\right) >$$

$$\cong -\rho C_f \left\{ < u' > < U_i U_i > + \left\langle \frac{u_i' u_j'}{u'} \right\rangle < U_i U_j > \right\} , \qquad (7)$$

provided $\vec{u}'$ and $\vec{U}$ are statistically independent. Since

$$< U_i U_j > = \frac{g^2 k_i k_j}{\omega^2 \cosh^2 kh} F(\vec{k}) \Delta\vec{k} \quad ,$$

where ω is frequency and h is water depth, Equation (7) becomes

$$\rho g \frac{\partial F(\vec{k})}{\partial t} = -\rho C_f \frac{g^2 k_i k_j}{\omega^2 \cosh^2 kh} F(\vec{k}) \left[\delta_{ij} < u > + \left\langle \frac{u_i u_j}{u} \right\rangle\right] \quad , \qquad (8)$$

by applying $\vec{u}' \cong \vec{u}$.

In Equation (8), if the current is zero, then

$$< u > = \int_{-\infty}^{\infty} u\, p(u)\, du$$

$$= \int_{-\infty}^{\infty} \int_{-\infty}^{\infty} \sqrt{u_1^2 + u_2^2}\, p(u_1, u_2)\, du_1\, du_2 \quad , \qquad (9)$$

where p is the probability density function, u_1 and u_2 are two orthogonal components of u. The coordinate system is chosen such that $< u_1\, u_2 > = 0$ and $< u_2^2 > < < u_1^2 >$. From the Gaussian property of wave field, the probability density function,

$$p(u_1, u_2) = \frac{1}{2\pi\, \sigma_1\, \sigma_2} \exp\left[- \frac{u_1}{2\sigma_1^2} - \frac{u_2}{2\sigma_2^2} \right] \quad , \qquad (10)$$

is obtained by applying $< u_1\, u_2 > = 0$, where $\sigma_1^2 = < u_1^2 >$ and $\sigma_2^2 = < u_2^2 >$. Applying Equation (10), Equation (9) becomes

$$< u > = \sqrt{\frac{2\sigma_1^2}{\pi}}\ E\left(\sqrt{1 - \frac{\sigma_2^2}{\sigma_1^2}} \right) ,$$

where E is the complete elliptic integral of the first kind. Using the same procedures, it can be found that

$$\frac{u_1^2}{u} = \frac{\sqrt{\frac{2\sigma_1^2}{\pi}}}{1 - \frac{\sigma_2^2}{\sigma_1^2}} \left[E\left(\sqrt{1 - \frac{\sigma_2^2}{\sigma_1^2}} \right) - \frac{\sigma_2^2}{\sigma_1^2} K\left(\sqrt{1 - \frac{\sigma_2^2}{\sigma_1^2}} \right) \right] ,$$

$$\left\langle \frac{u_2^2}{u} \right\rangle = \frac{\sqrt{2\sigma_1^2}}{\pi} \frac{\sigma_2^2}{\sigma_1^2} \left[K\left(\sqrt{1 - \frac{\sigma_2^2}{\sigma_1^2}} \right) - E\left(\sqrt{1 - \frac{\sigma_2^2}{\sigma_1^2}} \right) \right] \Bigg/ \left(1 - \frac{\sigma_2^2}{\sigma_1^2} \right) ,$$

and

$$\left\langle \frac{u_1 u_2}{u} \right\rangle = 0 ,$$

where K is the complete elliptic integral of the second kind.

LIST OF REFERENCES

1. Bagnold, R. A., 1946: Motion of waves in shallow water: Interaction between waves and sand bottoms. Proc. R. Soc. London, A187, 1-15.

2. Barnett, T. P., 1966: On the generation, dissipation, and prediction of ocean wind waves. Ph.D. dissertation, U.C. San Diego.

3. Barnett, T. P., 1968: On the generation, dissipation, and prediction of wind waves. J. Geophys. Res., 73, 513-530.

4. Barnett, T. P. and J. C. Wilkerson, 1967: On the generation of ocean wind waves as inferred from airborne radar measurements of fetch-limited spectra. J. Marine Res., 25, 292-328.

5. Bea, R. G., 1974: Gulf of Mexico hurricane wave heights. Proc. 6th Offshore Tech. Conf., OTC 2110, Dallas, Texas.

6. Benjamin, T. B., 1959: Shearing flow over a wavy boundary. J. Fluid Mech., 6, 161-205.

7. Benney, D. J., 1962: Nonlinear gravity wave interactions. J. Fluid Mech., 14, 577-584.

8. Breeding, J. E., Jr., 1972: Refraction of gravity water waves. Naval Coastal Systems Lab., Rep. NCSL 124-72, 161 pp.

9. Bretherton, F. P., 1964: Resonant interactions between waves. J. Fluid Mech., 20, 457-480.

10. Bretschneider, C. L., 1951: Revised wave forcasting curves and procedures. Unpublished Manuscript, Inst. Eng. Res., U.C. Berkeley, Cal.

11. Bretschneider, C. L., 1954: Generation of wind waves over a shallow bottom. Tech. memo., Beach Erosion Board, U.S. Army Corps of Engineers, No. 51, 24 pp.

12. Bretschneider, C. L., 1958: Revisions in wave forecasting; deep and shallow water. Proc. 6th Coastal Eng. Conf., ASCE.

13. Bretschneider, C. L., 1959: Wave variability and wave spectra for wind-generated gravity waves. Tech. memo., Beach Erosion Board, U.S. Army Corps of Engineers, No. 118, 192 pp.

14. Bretschneider, C. L. and R. O. Reid, 1954: Changes in wave height due to bottom friction, percolation, and refraction. Tech. memo., Beach Erosion Board, U.S. Army Corps of Engineers, No. 45, 36 pp.

15. Burling, R. W., 1959: The spectrum of waves at short fetches. Dtsch. Hydrogr. Zr., XII, 45-117.

16. Cardone, V. J., W. J. Pierson, and E. G. Ward, 1976: Hindcasting the directional spectra of hurricane-generated waves. J. Petroleum Tech., 28, 385-394.

17. Carpenter, S. H., L. J. Thompson, and W. R. Bryant, 1973: Visco-elastic properties of marine sediments. Proc. 5th Offshore Tech. Conf., OTC 1903, Dallas, Texas.

18. Carstens, M. R., F. M. Neilson, and H. D. Altinbilek, 1969: Bed forms generated in the laboratory under an oscillatory flow: analytical and experimental study. Tech. memo., Coastal Eng. Res. Center, U.S. Army Corps of Engineers, No. 28, 105 pp.

19. Collins, J. I., 1972: Prediction of shallow-water spectra. J. Geophys. Res., 77, 2693-2707.

20. Darbyshire, J., 1955: An investigation of storm waves in the north Atlantic Ocean. Proc. R. Soc. London, A230, 560-569.

21. Darbyshire, J., 1959: Further investigation of wind generated waves. Dtsch. Hydrogr. Zr., XII, 1-13.

22. Davis, R. E., 1970: On the turbulent flow over a wavy boundary. J. Fluid Mech., 42, 721-731.

23. Davis, R. E., 1972: On prediction of the turbulent flow over a wavy boundary. J. Fluid Mech., 52, 287-306.

24. Dingler, J. R., 1975: Wave-formed ripples in near shore sands. Ph.D. dissertation, U.C. San Diego.

25. Dobson, F. W., 1971: Measurements of atmospheric pressure on wind-generated sea waves. J. Fluid Mech., 48, 91-127.

26. Dobson, F. W. and J. A. Elliott, 1977: Wave-pressure correlation measurements over growing sea waves with a wave follower and fixed-height pressure sensors. NATO Symp. on Turb. Fluxes through the Sea Surface, Wave Dyn. and Prediction, Marseille, France.

27. Doyle, E. H., 1973: Soil-wave tank studies of marine soil instability. Proc. 5th Offshore Tech. Conf., OTC 1901, Dallas, Texas.

28. Elliott, J. A., 1972: Microscale pressure fluctuations near waves being generated by the wind. J. Fluid Mech., 54, 427-448.

29. Ewing, J. A., 1971: A numerical wave prediction method for the North Atlantic Ocean. Dtsch. Hydrogr. Zr., 24, 241-261.

30. Fox, M. J. H., 1976: On the nonlinear transfer of energy in the peak of a gravity-wave spectrum. II. Proc. R. Soc. London, A348, 467-483.

31. Gade, H. G., 1958: Effects of a nonrigid, impermeable bottom on plane surface waves in shallow water. J. Marine Res., 16, 61-82.

32. Gade, H. G., 1959: Notes on the effect of elasticity of bottom sediments to the energy dissipation of surface waves in shallow water. Archiv for Mathematik og Naturvidenskab, B. LV., Nr. 3, 69-80.

33. Gent, P. R. and P. A. Taylor, 1976: A numerical model of the air flow above water waves. J. Fluid Mech., 77, 105-128.

34. Hasselmann, K., 1962: On the non-linear energy transfer in a gravity-wave spectrum, Part 1. General theory. J. Fluid Mech., 12, 481-500.

35. Hasselmann, K., 1963a: On the non-linear energy transfer in a gravity wave spectrum, Part 2. Conservation theorems; wave-particle analogy; irreversibility. J. Fluid Mech., 15, 273-281.

36. Hasselmann, K., 1963b: On the nonlinear energy transfer in a gravity wave spectrum, Part 3. Evaluation of the energy flux and swell-sea interaction for a Neumann spectrum. J. Fluid Mech., 15, 385-398.

37. Hasselmann, K., 1968: Weak-interaction theory of ocean waves. In: Basic developments in fluid dynamics (Ed. M. Holt). New York. 2, 117-182.

38. Hasselmann, K., 1971: On the mass and momentum transfer between short gravity waves and larger-scale motions. J. Fluid Mech., 50, 189-205.

39. Hasselmann, K., 1974: On the spectral dissipation of ocean waves due to white capping. Boundary-Layer Meteor., 6, 107-127.

40. Hasselmann, K. and J. I. Collins, 1968: Spectral dissipation of finite-depth gravity waves due to turbulent bottom friction. J. Marine Res., 26, 1-12.

41. Hasselmann, K., T. P. Barnett, E. Bouws, H. Carlson, D. E. Hasselmann, P. Kruseman, A. Meerburg, P. Müller, D. J. Olbers, K. Richter, W. Sell, and H. Walden, 1973: Measurements of wind-wave growth and swell decay during the Joint North Sea Wave Project (JONSWAP). Dtsch. Hydrogr. Zr., Suppl. A, 8, No. 12.

42. Hasselmann, K., D. Ross, P. Müller, and W. Sell, 1976: A parametric wave prediction model. J. Phys. Oceanogr., 6, 200-228.

43. Herterich, K. and K. Hasselmann, 1978: A similarity relation for the nonlinear energy transfer in a finite-depth gravity-wave spectrum. submitted to J. Fluid Mech.

44. Inman, D. L., 1957: Wave-generated ripples in nearshore sands. Tech. memo., Beach Erosion Board, U.S. Army Corps of Engineers, No. 100, 65 pp.

45. Inoue, T., 1967: On the growth of the spectrum of a wind generated sea according to a modified Miles-Phillips mechanism and its application to wave forecasting. Dept. Meteor. & Oceanogr., NYU, TR 675, 74 pp.

46. Jonsson, I. G., 1965: Friction factor diagram for oscillatory boundary layers. Progr. Rep., Tech. Univ. Denm., No. 10, 10-21.

47. Jonsson, I. G., 1966: Wave boundary layers and friction factors. Proc. 10th Coastal Eng. Conf., ASCE.

48. Kamphuis, J. W., 1975: Friction factor under oscillatory waves. Proc. ASCE, 101, WW 2, 135-144.

49. Kolsky, H., 1963: Stress waves in solids (2nd edition). N.Y., Dover.

50. Lazanoff, S. M., N. M. Stevenson, and V. J. Cardone, 1973: A Mediterranean Sea wave spectral model. Tech. note, Fleet Num. Weather Cen., No. 73-1, 83 pp.

51. Lighthill, M. J., 1962: Physical interpretation of the mathematical theory of wave generation by wind. J. Fluid Mech., 14, 385-398.

52. Longuet-Higgins, M. S., 1962: Resonant interactions between two trains of gravity waves. J. Fluid Mech., 12, 321-332.

53. Longuet-Higgins, M. S., 1969: A nonlinear mechanism for the generation of sea waves. Proc. R. Soc. London, A311, 371-389.

54. Longuet-Higgins, M. S., 1976: On the nonlinear transfer of energy in the peak of a gravity-wave spectrum: a simplified model. Proc. R. Soc. London, A347, 311-328.

55. Longuet-Higgins, M. S. and O. M. Phillips, 1962: Phase velocity effects in tertiary wave interactions. J. Fluid Mech., 12, 333-336.

56. Longuet-Higgins, M. S. and N. D. Smith, 1966: An experiment on third order resonant wave interactions. J. Fluid Mech., 25, 417-435.

57. McGoldrick, L. F., O. M. Phillips, N. Huang, and T. Hodgson, 1966: Measurements on resonant wave interactions. J. Fluid Mech., 25, 437-456.

58. McLeroy, E. G., 1972: Measurement and correlation of acoustic reflection and sediment properties off Panama City, Florida. Naval Coastal Systems Lab., Informal Rep. NCSL 112-72, 20 pp.

59. Mallard, W. W. and R. A. Dalrymple, 1977: Water waves propagating over a deformable bottom. Proc. 9th Offshore Tech. Conf., OTC 2895, Houston, Texas.

60. Meisburger, E. P. and M. E. Field, 1975: Geomorphology, shallow structure, and sediments of the Florida inner continental shelf, Cape Canaveral to Georgia. Tech. Memo., Coastal Eng. Res. C., U.S. Army Corps of Engineers, No. 54, 119 pp.

61. Migniot, C., 1968: A study of the physical properties of various forms of very fine sediment and their behaviors under hydrodynamic action. La Houille Blanche, 7, 591-620.

62. Miles, J. W., 1957: On the generation of surface waves by shear flows. J. Fluid Mech., 3, 185-204.

63. Miles, J. W., 1959: On the generation of surface waves by shear flows, Part 2. J. Fluid Mech., 6, 568-582.

64. Miles, J. W., 1960: On the generation of surface waves by turbulent shear flows. J. Fluid Mech., 7, 469-478.

65. Miles, J. W., 1967: On the generation of surface waves by shear flows, Part 5. J. Fluid Mech., 30, 163-175.

66. Mitsuyasu, H., 1968: A note on the nonlinear energy transfer in the spectrum of wind-generated waves. Rep. Res. Inst. Appl. Mech., Kyushu Univ., 16, 251-264.

67. Mogridge, G. R. and J. W. Kamphuis, 1972: Experiments on bed form generation by wave action. Proc. 13th Coastal Engng. Conf., ASCE, 1123-1142.

68. Neumann, G., 1953: On ocean wave spectra and a new method of forecasting wind-generated sea. Tech. memo., Beach Erosion Board, U.S. Army Corps of Engineers, No. 43.

69. Phillips, O. M., 1957: On the generation of waves by turbulent wind. J. Fluid Mech., 2, 417-445.

70. Phillips, O. M., 1958: The equilibrium range in the spectrum of wind generated waves. J. Fluid Mech., 4, 426-434.

71. Phillips, O. M., 1960: On the dynamics of unsteady gravity waves of finite amplitude. Part 1. J. Fluid Mech., 9, 193-217.

72. Phillips, O. M., 1963: On the attenuation of long gravity waves by short breaking waves. J. Fluid Mech., 16, 321-332.

73. Phillips, O. M., 1969: The dynamics of the upper ocean. Cambridge University Press.

74. Pierson, W. J. and L. Moskowitz, 1964: A proposed spectral form for fully developed wind seas based on the similarity theory of S. A. Kitaigorodskii. J. Geophys. Res., 69, 5181-5190.

75. Pierson, W. J., G. Neumann, and R. W. James, 1955: Observing and forecasting ocean waves by means of wave spectra and statistics. Hydrographic Pub. 603, U.S. Navy Dept.

76. Pierson, W. J., L. J. Tick, and L. Baer, 1966: Computer based procedures for preparing global wave forecasts and wind field analysis capable of using wave data obtained by a spacecraft. Proc. 6th Symp. Naval Hydrodyn., Washington, D.C.

77. Putnam, J. A., 1949: Loss of wave energy due to percolation in a permeable sea bottom. Trans. Amer. Geophys. Un., 30, 349-356.

78. Putnam, J. A., and J. W. Johnson, 1949: The dissipation of wave energy by bottom friction. Trans. Amer. Geophys. Un., 30, 67-74.

79. Reynolds, W. C. and A. K. M. F. Hussain, 1972: The mechanics of an organized wave in turbulent shear flow. Part 3. Theoretical models and comparisons with experiments. J. Fluid Mech., 54, 263-288.

80. Roll, H. U. and G. Fisher, 1956: Eine Kritische Bemerkung Zum Neumann-Specktrum der Seeganger. Dtsch Hydrogr. Zr., IX, 9-14.

81. Rosenthal, W., 1978: Energy exchange between surface waves and motion of sediment. J. Geophys. Res., 83, 1980-1982.

82. Salfi, R. E., 1974: Operational computer based spectral wave specification and forecasting models. Univ. Inst. Oceanogr., CUNY.

83. Scott, J. R., 1965: A sea spectrum for model tests and long-term ship prediction. J. Ship Res., Dec. 1965, 145-152.

84. Sell, W. and K. Hasselmann, 1972: Computations of nonlinear energy transfer for JONSWAP and empirical wind wave spectra. Inst. Geophys., Univ. Hamburg.

85. Shemdin, O. H., 1969: Instantaneous velocity and pressure measurements above propagating waves. Tech. Rep., Dept. of Coastal & Oceanogr. Eng., U. Florida, No. 4.

86. Shemdin, O. H., J. E. Blue, and J. A. Dunne, 1975: SEASAT-A surface truth program, Marineland test plan. Jet Propulsion Lab., 622-5.

87. Shemdin, O. H., K. Hasselmann, S. V. Hsiao, and K. Herterich, 1977: Nonlinear and linear bottom interaction effects in shallow water. NATO Symp. on Turb. Fluxes through the Sea Surface, Wave Dyn. and Prediction, Marseille, France.

88. Skovgaard, O., I. G. Jonsson, and J. A. Bertelsen, 1975: Computation of wave heights due to refraction and friction. Proc. ASCE, 101, WW1, 15-32.

89. Sleath, J. F. A., 1970: Wave-induced pressures in beds of sand. Proc. ASCE, 96, HY 2, 367-378.

90. Snyder, R. L., 1974: A field study of wave-induced pressure fluctuations above surface gravity waves. J. Marine Res., 32, 497-531.

91. Snyder, R. L. and C. S. Cox, 1966: A field study of the wind generation of ocean waves. J. Marine Res., 24, 141-178.

92. Synder, R. L., R. B. Long, F. W. Dobson, and J. A. Elliott, 1977: The Bight of Abaco pressure experiment. NATO Symposium on Turb. Fluxes through the Sea Surface, Wave Dyn. and Prediction, Marseille, France.

93. Suhayda, J. N., T. Whelan, J. M. Coleman, J. S. Booth, and L. E. Garrison, 1976: Marine sediment instability: interaction of hydrodynamic forces and bottom sediments. Proc. 8th Offshore Tech. Conf., OTC 2426, Dallas, Texas.

94. Sverdrup, H. U. and W. H. Munk, 1947: Wind, sea and swell: theory of relations for forecasting. Hydrogra. Office Pub. 601, U.S. Navy Dept.

95. Tolbert, W. H. and G. B. Austin, 1959: On the nearshore marine environment of the Gulf of Mexico at Panama City, Florida. Naval Coastal System Lab., Rep. TP 161.

96. Townsend, A. A., 1972: Flow in a deep turbulent boundary layer over a surface distorted by water waves. J. Fluid Mech., 55, 719-735.

97. Tubman, M. W. and J. N. Suhayda, 1976: Wave action and bottom movements in fine sediments. Proc. 15th Coastal Eng. Conf., ASCE.

98. U.S. Army Coastal Engineering Research Center, 1973: Shore protection manual. Dept. of the Army, Corps of Engineers.

99. Van Ieperen, M. P., 1975: The bottom friction of the sea-bed off Melkbosstrand, South Africa: a comparison of a quadratic with a linear friction model. Dtsch. Hydrogr. Zr., 28, 72-88.

100. Willebrand, J., 1975: Energy transport in a nonlinear and in homogeneous random gravity wave field. J. Fluid Mech., 70, 113-126.

BIOGRAPHICAL SKETCH

Shu-Chi Vincent Hsiao was born 19 October 1948 in Shanghai, China. He received his BS in Civil Engineering in 1970 and his MS in Civil Engineering in 1972 from National Taiwan University, Taipei, Taiwan. He entered the School of Marine Science, College of William and Mary, Williamsburg, Virginia in 1973. In 1974 he transferred to the University of Florida to begin his study in Coastal and Oceanographic Engineering.

I certify that I have read this study and that in my opinion it conforms to acceptable standards of scholarly presentation and is fully adequate, in scope and quality, as a dissertation for the degree of Doctor of Philosophy.

Omar H. Shemdin

O. H. Shemdin, Chairman
Professor of Coastal and Oceanographic Engineering

I certify that I have read this study and that in my opinion it conforms to acceptable standards of scholarly presentation and is fully adequate, in scope and quality, as a dissertation for the degree of Doctor of Philosophy.

Martin O. E.

M. A. Eisenberg
Professor of Engineering Sciences

I certify that I have read this study and that in my opinion it conforms to acceptable standards of scholarly presentation and is fully adequate, in scope and quality, as a dissertation for the degree of Doctor of Philosophy.

U. H. Kurzweg

U. H. Kurzweg
Professor of Engineering Sciences

I certify that I have read this study and that in my opinion it conforms to acceptable standards of scholarly presentation and is fully adequate, in scope and quality, as a dissertation for the degree of Doctor of Philosophy.

C. P. Luehr

C. P. Luehr
Associate Professor of Mathematics

I certify that I have read this study and that in my opinion it conforms to acceptable standards of scholarly presentation and is fully adequate, in scope and quality, as a dissertation for the degree of Doctor of Philosophy.

K. Millsaps
Professor of Engineering Sciences

This dissertation was submitted to the Graduate Faculty of the College of Engineering and to the Graduate Council, and was accepted as partial fulfillment of the requirements for the degree of Doctor of Philosophy.

Hubert A. Bevis
Dean, College of Engineering

Dean, Graduate School